UNIVERSITY OF BIRMINGHAM


**Department of Metallurgy & Materials**

# Irradiation Damage Simulations of Platinum Group Metal Modified Austenitic Stainless Steels for Reactor Core Components

by Ben Palmer

A thesis submitted to the University of Birmingham for the degree of Doctor of Philosophy

Supervised by Dr Brian J Connolly and Dr Mark S D Read

**Irradiation Damage Simulations of Platinum Group Metal Modified Austenitic Stainless Steels for Reactor Core Components**

by

Ben Palmer

**Abstract**

*T*his work is split into two investigations. The first focuses on deriving the interatomic potentials required to model irradiated austenitic stainless steels doped with small amounts of Palladium or Ruthenium. The second centers on a Fortran program developed to predict the radioactivity of a sample irradiated by a proton beam.

Austenitic stainless steels are an important material, and it is used to construct core components within nuclear reactors. Sensitisation of these steels, by processes such as welding, depletes Chromium from grain boundaries removing the corrosion resistant $Cr_2O_3$ passive layer. Previous (experimental) work has shown that these steels, when doped with palladium or ruthenium, retain corrosion resistance at the grain boundary. This work investigates whether or not these PGMs deplete or saturate at the grain boundary while under irradiation using Molecular Dynamics (MD) simulations. Interatomic potentials have been derived for Fe-Pd and Fe-Ru as they were not available, and these are essential for the MD simulations of the irradiated grain boundaries. The effect of irradiation on Fe-Ru and Fe-Pd showed depletion/saturation/no effect.

In addition to simulations, it would also be desireable to investigate whether PGMs are depleted or saturated at the grain boundary by emulating neutron damage with a proton beam. The irradiated targets are expected to be radioactive due to the transmutation of target nucleons. A Fortran program, Activity, was written and developed to calculate how radioactive a target sample would be after proton beam irradiation, and from this it can be determined when it would be safe to handle.

# Contents

# List of Figures

# List of Tables

# Chapter 1

# Introduction

*Several generation III+ nuclear reactors have been proposed for construction in the UK and generation IV nuclear reactors being researched and developed. New materials are required to withstand the extreme conditions in and around the core of these reactors. Austenitic stainless steels have been an important structural material in the industry, and may continue to be so, providing the problem of Intergranular Stress Corrossion Cracking (IGSCC) can be addressed. Doping these steels with platinum group metals has been seen to reduce IGSCC, but the effects are unknown for these steels in a radiation field.*

# Nuclear Power in the UK

Magnox type reactors were the first used in the United Kingdom. These reactors used natural Uranium as a fuel and were carefully designed to produce energy despite using an unenriched fuel. Graphite was used as a moderator, and the low neutron capture cross section of the Magnox cladding allowed th

## Generation 1 Reactors

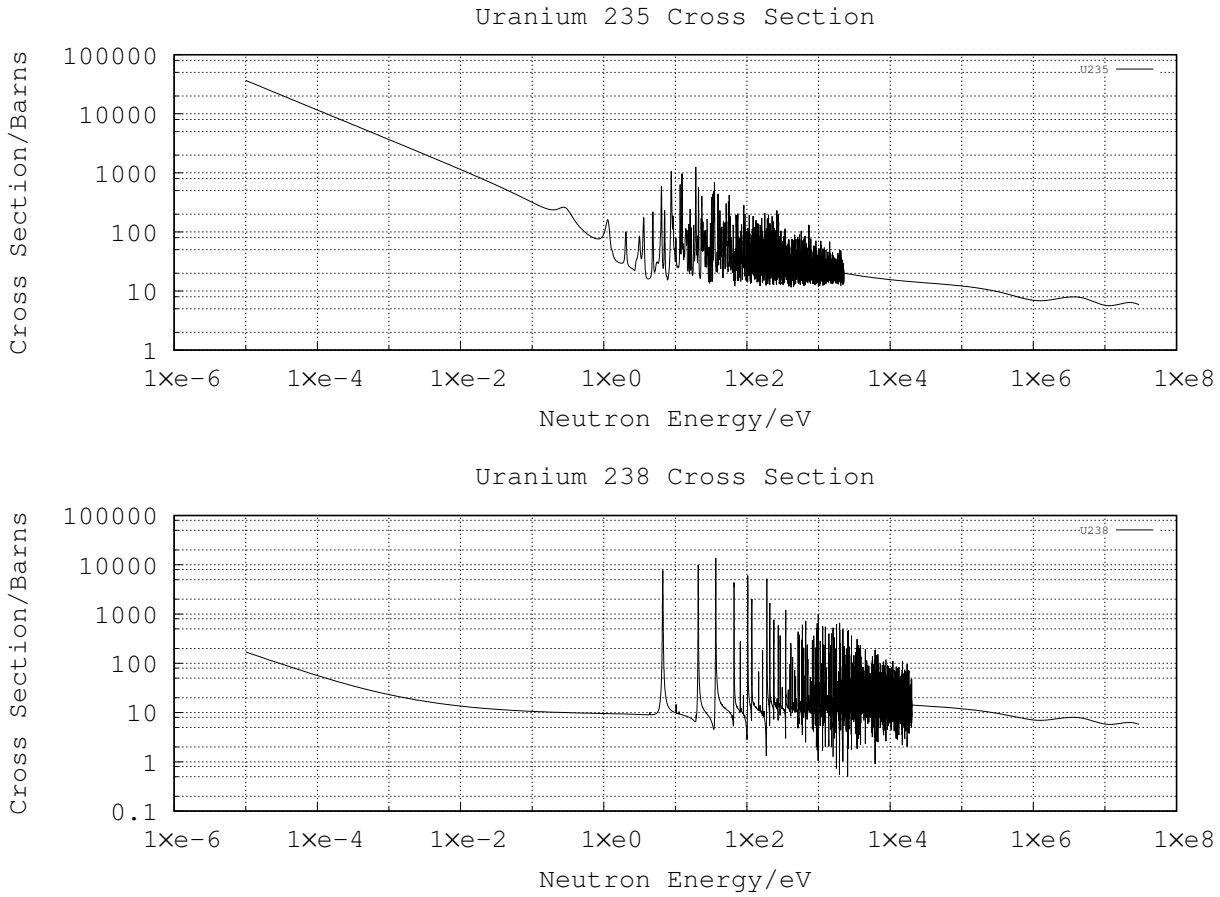


Figure 1.1: Graph caption

## Generation 2 Reactors

## Generation 3 Reactors

# An Approaching Energy Gap for the UK

Since Calder Hall, the first commercial nuclear power plant, opened in 1956, the demand on electrical power generation in the UK has tripled. There is now a reliance on cheap and clean power from nuclear reactors as these provide a quarter of our electricity. There are sixteen reactors operational in the UK: the Magnox reactor at Wylfa and the fourteen AGR reactors are due to be decommissioned by 2023[1], and the remaining PWR reactor, Sizewell B, is expected to remain operational until 2035[1].

There is an obvious concern that within the next ten years the UK will lose a sizeable proportion of its electricity generation capabilities, however, there are proposals to remedy this. EDF have planned to build two new reactors

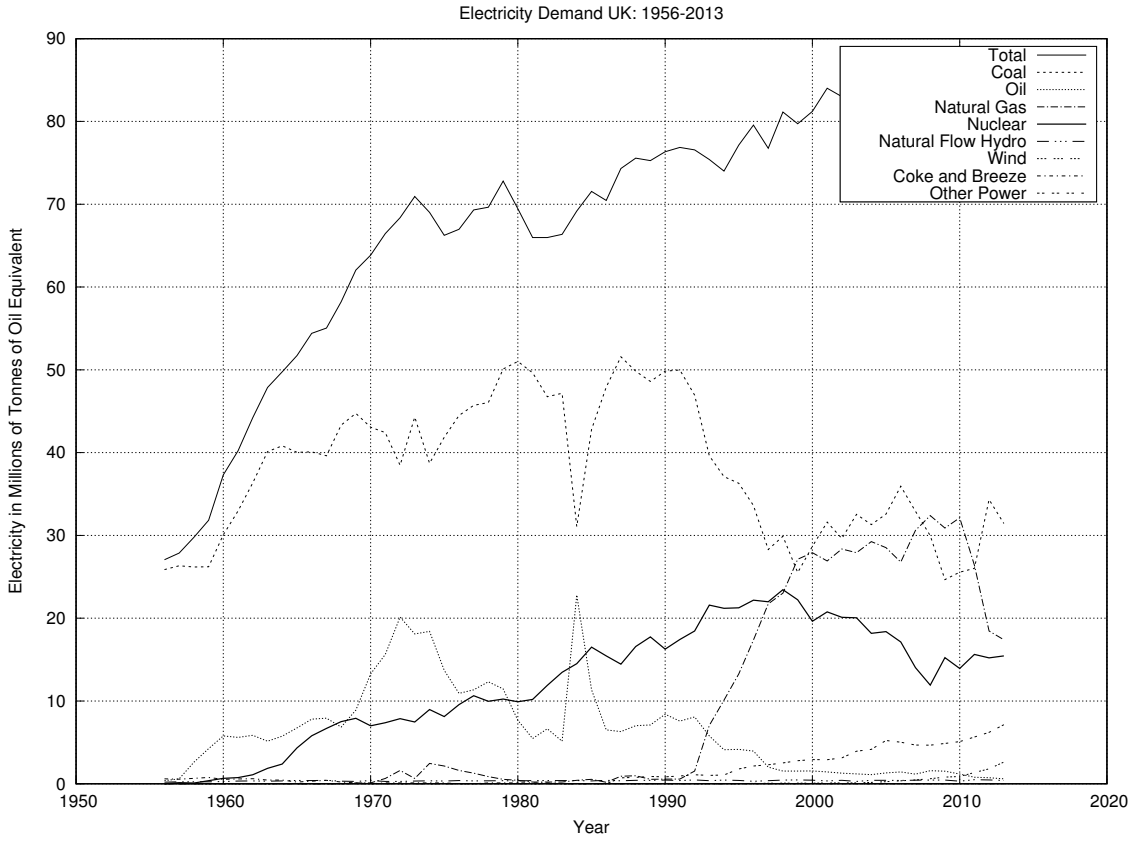


*Figure 1.2: Electricity in Millions of Tonnes of Oil Equivalent*

at the Hinkley Point site in Somerset. Hinkley Point C will contain two Areva NP designed Gen III+ EPR reactors. Many advanced materials, including a variety of types of Austenitic Stainless Steel, will be used in the construction of these reactors.

The physical stresses subjected to the Gen IV reactors will go beyond those that are currently being built. There will be higher radiation doses and faster, more damaging neutrons. Coolant temperatures will be higher to either give better thermodynamic efficiency or open the route to creating hydrogen directly as a fuel. Novel coolants such as lead and sodium, each with their own challenges to overcome, are also being considered.

## Proposed Generation III+ Nuclear Power Plants

Although work has not started, at the time of writing, several sites have been acquired with the aim of building new nuclear power stations. There are five sites and three reactor designs[2]:

- Hinkley Point: two Areva EPRs (EDF Energy)
- Sizewell: two Areva EPRs (EDF Energy)
- Wylfa: 2-3 Hitachi ABWRs (Horizon Nuclear Power)
- Oldbury: 2-3 Hitachi ABWRs (Horizon Nuclear Power)
- Sellafield: 3 Westinghouse AP1000s (NuGeneration) ...

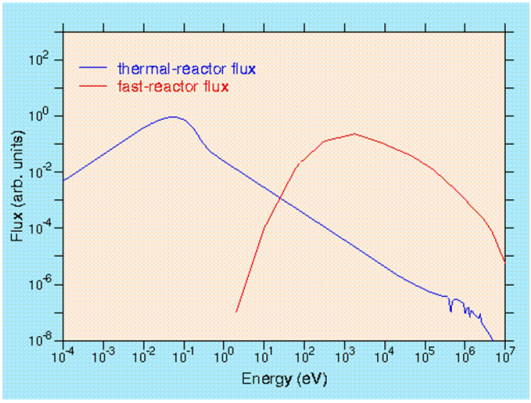


Figure 1.3: Graph caption

**EPR**

**AP1000**

## Generation IV Proposed Designs

### Super-Critical Water Reactors (SCWR)

Supercritical water exists above 374oC and 22.1MPa, and in this state water has a higher thermodynamic efficiency. The design of the nuclear power plant is also simplified as there is no phase change of the water, so a condenser is not needed. The SCWR is the only GEN IV reactor design that uses water as the coolant[1]. The economic benefits have already been seen in SCW fossil fuel power stations, and it is incorporated in GenIV water cooled fast and thermal reactors. The combination of supercritical water chemistry and irradiation damage must be considered, as well as higher temperature and pressure.

PWR 288-325oC 15.2 MPa[2]

BWR 278-287oC 7.1MPa[3]

### Lead-cooled Fast Reactors

One example of the next generation reactor designs is ELSY: the European Lead Fast Reactor. It is a fast neutron reactor and this benefits from a lead coolant as lead has a low reaction cross section and the maximum energy lost per neutron-coolant atom collision is low. The Lead coolant will be at a temperature of 400oC to 480oC[4] and will weigh 9,000 tons. The challenge for engineers is to develop materials that can survive such extreme conditions, including the corrosiveness of the liquid lead and the high flux of fast neutrons. (5).

### Gas Cooled Fast Reactors

Very high outlet temperatures can be achieved for GFRs, with the temperature of the gas coolant ranging from 490oC to 850oC (6) and this requires advanced materials that can withstand temperatures as high while under high energy neutron flux. Unlike LFRs and SCWRs, the coolant is inert, leaving engineers to overcome high temperatures and irradiation damage.

### Experimental Fusion Reactors

Nuclear Fusion is a very attractive technology and could be the answer to all of our energy problems. Much work is being invested in developing this technology and the ITER (International Thermonuclear Experimental Reactor) has been designed to output more energy than is required to start the fusion reaction. The process of fusion combines two isotopes of hydrogen and leaves helium and fast neutrons. As neutrons have no charge, they can penetrate shielding causing damage as they lose energy through nuclear interactions. Any atoms they interact with have a chance to capture the neutron and become unstable.

$$ {}_1D^2 +_1 T^3 \rightarrow_2 He^4(3.5MeV) +_0 n^2(14.1MeV) \tag{1.1} $$

The fast neutron spectrum for fission reactors ranges from a few eV to a few MeV, whereas the neutrons in a fusion reaction have 2-3 times more energy than the most energetic neutrons from fast fission. Engineers must develop materials to construct components that will be resilient to this damage, while having a low reaction cross section and being able to withstand other extreme conditions within the reactor.

## Materials Developed for Nuclear Power

With temperatures of several hundred degrees or more, pressures exceeding 150 atomspheres and a high levels of irradiation, $1.0x10^{1}1$ neutrons per "$cm$"$^{2}$ per second, the interior of a nuclear reactor is a hostile and damaging environment. The choice of material is further complicated due to a number of factors.

- Isotopes with a high neutron capture cross section that poison the reactor (Xenon-135 and Samarium-149)
- Limiting creation of hazardous radioactive material in the structural material of the reactor (Cobalt-60)
- Absorbtion of neutrons by structual material

The environment within the reactor is due to become more hostile as future reactor designs are developed. A number of reactors will operate at higher temperatures (850 degrees or more) while others are being designed to replace water as a coolant with liquid metal salts.

# Austenitic Stainless Steel and Reactors

## Stainless Steels

The defining feature of a stainless steel is a Chromium content of more than 10.5

### Passive Film Protection of Chromium

Chromium improves the resistance of stainless steel by forming a passive oxide layer Cr2O3. Chromium atoms and chromium oxide are similar in size, so they pack well into the crystal structure of the steel. The resistance of austenitic stainless steels can be improved further by added other elements, and removing some impurities (or elements found in other standard compositions). Read: nature of passive films  McBee, Kruger

### Ferritic Stainless Steel

Ferritic stainless steels have a crystal structure similar to pure Iron at room temperature which is bcc. These steels are magnetic and may be hardened by cold working. They are less corrosion resistant than austenitic stainless steels. Two common examples of this grade of steel are ASME (American Society of Mechanical Engineers) codes 405 and 430.

### Martensitic Stainless Steel

### Duplex Stainless Steel

### Austenitic Stainless Steel

Austenite is a FCC allotrope of Iron, and austenitic stainless steels are useful in many applications, including a structural material for nuclear plant components, due to their resistance to corrosion. In addition to 11 wt

Two examples of such steels are ASME codes 304 and 316. Both have a high Chromium content, in the region of 18-20

Unlike Austenitic and Ferritic, Martensitic stainless steels can be heat treated to harden the steel. These steels are magnetic and have a FCT crystal structure. They contain more than 10.5

## Austenitic Stainless Steels in the Nuclear Industry

Low cobalt content

## Issues Associated with Austenitic Stainless Steels

### Chromium Sensitization

When steels with Chromium content are heated, during processes such as welding, the metal undergoes Chromium sensitization. On heating to temperatures between 600-700oC for many hours Chromium carbides, of the form M23C6, are created, depleting Chromium at the grain boundary.

Steel held at elevated temperatures Chromium carbides precipitate at grain boundary Depletes the grain boundary of chromium Models of Tedmon et al, Fullman or Stawstrom and Hillert Difficult to model, depends on grain structure, intergranular carbide spacing

### Intergranular Stress Corrosion Cracking

### Transgranular Stress Corrosion Cracking

# Chapter 2

# Literature Review

*Chapter Summary*

## Improving Resistance of Austenitic Stainless Steels to Intergranular Stress Corrosion Cracking

¡Intro¿

## Doping Alloys with Palladium and Ruthenium

The corrosion resistant benefits of small amounts of palladium (4) and ruthenium (5) have been investigated. Due to the high cost of both palladium and ruthenium, there has been much interest in finding the optimum percentage of both. Ru and Pd doped stainless steels would be worth the additional cost if their corrosive resistant properties are maintained at the grain boundary. In particular, ruthenium has been shown to be beneficial to stainless steels where chloride containing solutions are concerned (5). There have been a number of proposed mechanisms of how PGMs enhance the corrosion resistance of steel.

### Cathodic Modification

Cathodic modification is one method that has been known for the last century (6), and the inhibition of anodic dissolution of the stainless steel has also been studied (7). The layer of PGM adatoms, atoms on the crystal surface, block anodic sites within the crystal which stops corrosion attack local to the adatoms (1).

### Effect on Intergranular Stress Corrosion Cracking

### Other Notable Corrosion Resistance Enhancing Alloys

Molybednum has been added to these steels to improve the resistance of pitting corrosion (4), and it has been shown to improve resistance against chloride containing solutions. Enhancing Resistance to Corrosion

## Radiation Damage

¡intro¿

## Damage Event

## Neutron & Ion Irradiation Sources

## Target Irradiation

## Radiation Induced Segregation, Depletion and Precipitation

Work by Aust et al, Howard + Lidiard, Anthony et al, Okamato + Wiedersich

Inverse Kirkendall Effect

Solute Vacancy Drag Mechanism

Oversized and Undersized Solute Migration

2.3.5 Irradiation Assisted Stress Corrosion Cracking

# Chapter 3

# Scope of Work & Thesis Objectives

*Chapter Summary*

## Scope of Work

¡Intro¿

# Chapter 4

# Background: Proton Activation and Radioactive Decay

*Chapter Summary*

## Why

Cyclotron comparitively cheap etc

### Ion Irradiation at the University of Birmingham

The Scanditronix MC-40 Cyclotron is used at the University of Birmingham to create a beam of protons or other light ions. The energies of these ions are typically between 10 MeV and 60 MeV with beam currents ranging up to 50 microamps ($3.1x10^{14}$ protons per second). Target materials are irradiated by this cyclotron for a number of reasons, including purposely creating radioactive isotopes for the nearby Queen Elizabeth Hospital, investigating ion irradiation damage and emulating neutron irradiation.

The Cyclotron is usually used to create radioactive isotopes for medical use, but an additional beam line has been devoted to material science investigations into radiation damage. While the creation of radioactive isotopes is desired in some cases, material being tested for radiation damage should preferably have low levels of radioactivity.

It is expensive to arrange the irradiation of target materials by high energy neutrons sources, whereas it is relatively inexpensive to irradiate using an ion beam on the MC-40 Cyclotron. The energies can be controlled, and a set dose at a single energy, or a range of energies, can be precisely deposited into the target material.

The Activity code discussed here was developed to calculate the activity of a target material irradiated by a proton beam. It has been developed in Fortran and uses data from the TENDL-2013 proton cross section database, SRIM ion transport code and NDS radioactive decay database.

### Simulating Ion Irradiation with SRIM

A package of ion transport codes, SRIM, is freely available to download and use to investigate the transport of ions through matter. SRIM uses the binary collision approximation (BCA) to simulate the passage of ions in a material. It is an approximate method, and one key restriction is that it does not take into account the structure of the material, and this approximation is therefore also imposed on the Activity code.

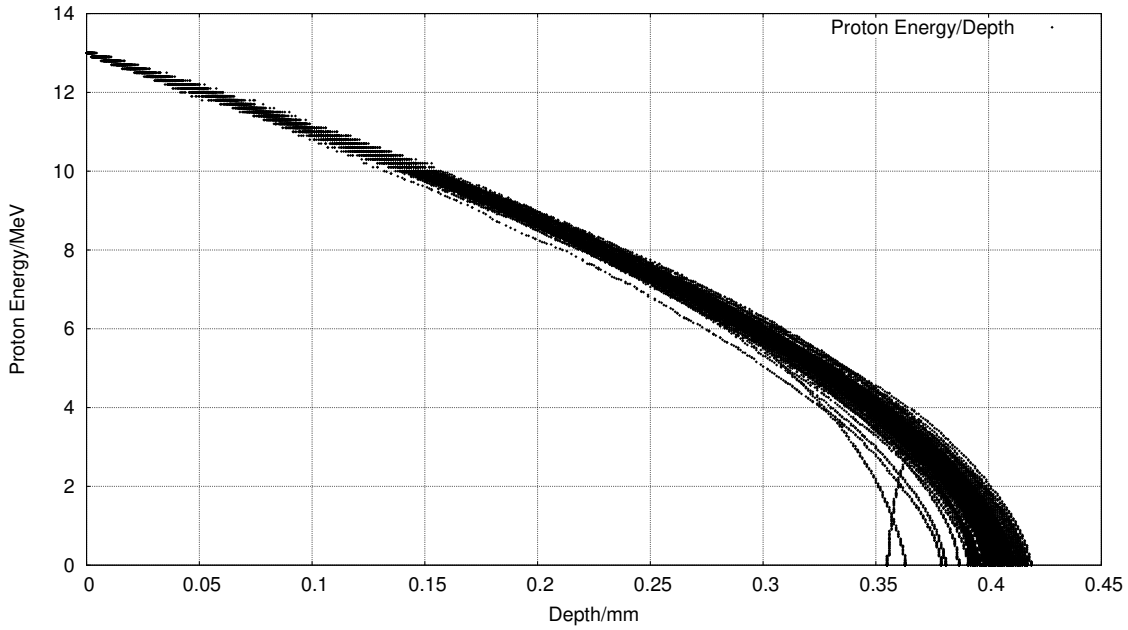


*Figure 4.1: One hundred simulated 13MeV proton energy loss curves in Fe simulated with SRIM [5]*

One file that SRIM creates is of importance to the Activity code, and that is the trajectory file that contains the energy and x,y,z co-ordinate data points for simulated ions moving through matter. Figure 4.1 shows the trajectory of one hundred 13MeV protons entering and passing through an Iron target, and it is this set of data points (together with the cross section database) that the Activity code uses to calculte the reaction rates for the transmutation of nuclei in the target. At higher energies, the ions slow as they lose energy due to electronic stopping, but as the ion energy drops the mechanism of loss through nuclear collisions becomes important. The spreading of ion depths at lower energies is a result of the higher momentum transfer during nuclear collisions, as can be seen in Figure 4.1.

## Transmutation of Nuclei by Ion Irradiation

Considering a simplified nuclear potential well, energetic protons approaching a nucleus may overcome the Coulomb potential barrier. They are captured by the nucleus and held within the potential well by the strong nuclear force. This process may leave the nucleus in an excited and unstable state, depending on the input energy of the proton and configuration of nucleons. The process is probabilistic, and the average chance of a reaction (the microscopic cross section) may be measured as a function of the projectile, projectile energy and target, either experimentally or by optical model potential calculations. The reaction rate is calculated from the microscopic cross section using the following equation:

$$R = \frac{J}{e} n_t \sigma \cdot 10^{-28} \delta t \tag{4.1}$$

- R Reaction Rate (reactions per second)
- J Beam current (A)
- $n_t$ Number density of target (atoms per cubic metre)
- $\sigma$ Microscopic reaction cross section (barns)
- e Elementary charge (1.602177E-19C)
- $\delta$T Target thickness (m)

## Radioactive Decay

Radioactive decay is the random change in nucleons or energy state of an unstable nucleus. It is impossible to predict when a single nucleus will decay, but the decay of a collection of nuclei is statistical in nature. The radioactivity and number of unstable nuclei at time t can be predicted using the decay constant, λ, for the radioactive isotope. This constant is defined as follows:

$$\lambda = -\frac{N'(t)}{N(t)} \tag{4.2}$$

The number of radioactive nuclei N(t) at time t is given by the following equation, where N(0) is the starting number of nuclei:

$$N(t) = N(0)\exp(-t\lambda) \tag{4.3}$$

The activity A(t) of the radioactive nuclei is predicted at time t by using the following equations, where N'(t) is the change in amount of nuclei with respect to time:

$$A(t) = -N'(t) = \lambda N(t) \tag{4.4}$$

$$A(t) = \lambda N(0)\exp(-t\lambda) \tag{4.5}$$

## Bateman Equation for Radioactive Decay

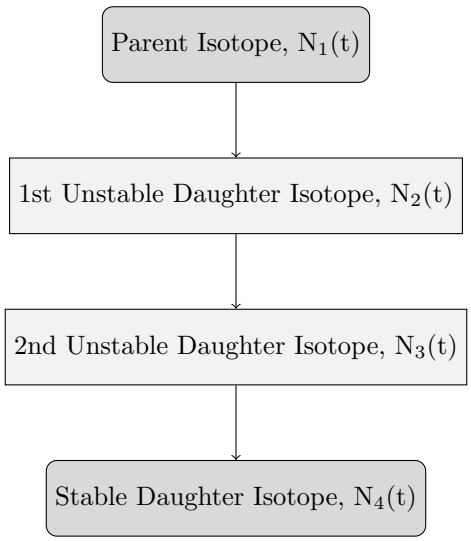


*Figure 4.2: An example decay chain from an unstable parent isotope, through unstable daughter isotopes ending with a stable daughter isotope.*

The English mathematician Harry Bateman derived an equation (4.6) to calculate the amount of each isotope in a decay chain, illustrated in Figure 4.2, at time t.

$$N_n(t) = \sum_{i=1}^{i=n}\left(\left(\prod_{j=i}^{j=n-1}\lambda_{(ij+1)}\right)\sum_{j=i}^{j=n}\left(\frac{N_{i0}\exp(-\lambda_j t)}{\prod_{p=i,p\neq j}^{p=n}(\lambda_p-\lambda_j)}\right)\right) \tag{4.6}$$

When a radioactive isotope decays, there may be more than one mode of decay, and this leads to branching factors. Pb-214 only decays via beta decay to Bi-214, giving a branching factor of 1.0, whereas Bi-214 has a

99.979% chance of decaying to Po-214 by beta decay and a 0.021% of emitting an alpha particle and decaying to Tl-210 (branching factors of 0.99979 and 0.00021 respectively) [6].

When a target material is irradiated, there is a source term for transmuted nuclei due to the irradiation. The daughter isotopes of these transmuted isotopes will also be affected by the irradiation and will transmute further, giving a source term for each daughter isotope as a result of the irradiation. Sources for each isotope in the decay chain, and branching factors between a parent isotope and its daughter isotope/s must be accounted for.

# Chapter 5

# Background: Interatomic Potential Fitting

*Chapter Summary*

## Experiment, Modelling and Theory

Experiment: direct answers from physical reality Limited by technology of the time, also limits due to Heisenberg uncertainty principle Theory: state of the art theories have been replaced numerous times in the past Quantum mechanics is a very accurate theory under certain circumstances Some problems just too hard to solve with these theories Modelling: bridges the gap Experiment and theory have their flaws, so does modelling Helps show what experiment cant, and where theory is too hard to solve Aim: take very accurate DFT calculations based on quantum theory, extrapolate to a larger scale by fitting EAM potentials, open a path to simulations of Pd + Fe and Ru + Fe

## Simulating Materials on a Variety of Scales in Time and Space

## Density Functional Theory

Density Functional Theory (DFT) is a branch of quantum chemistry that approximately solves the Schrdinger equation using electron density, rather than the coordinates of each electron in the system. There are many other simplifications that must be added in order for DFT to be practical to use, but despite this calculations are limited to just hundreds or thousands of atoms. A calculation of a hundred or so atoms may take thousands of CPU hours at the time of writing, depending on the type of calculation and complexity of the electron structures of the atoms involved.

It is through DFT that the first principles energy, stress and force calculations will be made, and it's these results that the EAM potentials will be trained and fit to using the force matching method. This will allow much larger scale modelling using the extrapolated behaviour of accurate DFT calculations.

### Brief Overview of DFT

Several important theories and approximations are used by DFT with the aim of calculating and minimising energies and forces. The Born-Oppenheimer approximation separates the electron-nucleus wave function. It

treats the nuclei as fixed points, and the system of electrons in a fixed potential created by the nuclei.

the DFT of Kohn, Sham and Hohenburg proved that the potential of a system is uniquely determined by its ground state density. This makes solving the Schrdinger equation significantly easier.

### Time Independent Schrdinger Equation

The Schrdinger equation of a system contains all the information about that system. For all but the simplest systems, it is a near impossible task to solve the Schrdinger equation.

# Classical Molecular Dynamics

# Kinetic Monte Carlo

# Interatomic Potentials

Classical molecular dynamics simulations are used to study small volumes of a material, with up to 107 atoms in a typical simulation. Such simulations have been used to model grain boundaries, and within these models irradiation damage may be simulated by initiating atom cascades that result from neutron radiation. Trautt and Mishin used molecular dynamics to study grain boundary migration in copper (12), and a more relevant example is the study by Shibuta et al and their model of grain boundary energy in bcc iron-chromium (13).

The temperature and pressure of the model can also be controlled, and this is important because there may be a temperature dependence on the rate of depletion of PGMs at the grain boundary, if there is depletion at all.

One key ingredient to any classical molecular dynamics simulation is the interatomic potential used to describe the forces between atoms in the model. Initially, simple pair potentials that described the force between two atoms were used.

2.6.1 Morse and Lennard Jones Pair Potentials

Early interatomic potentials were two-body pair potentials, where the force on an atom was determined by summing the pair potentials between that atom and other atoms in its neighbourhood, determined by a cutoff radius.

The Lennard-Jones and Morse potentials are examples of pair-potentials, but they are too simple. They cannot capture the many-body aspect of how atoms in a metal interact with each other. Many-body potentials such as the Finnis-Sinclair or Embedded Atom Model do have a pair potential function, and this can take the form of a LJ potential, Morse potential or other standard Pair Potentials.

$$U_{EAM} = \frac{1}{2}\sum_{i=1}^{N}\sum_{j\neq i}^{N} V_{ij}(r_{ij}) + \sum_{i=1}^{N} F[\rho_i] \qquad \text{where } \rho_i = \sum_{j=i, j\neq i}^{N} \rho_{ij}(r_{ij}) \tag{5.1}$$

Professor Howard Sheng created a website with many EAM potentials, and the plots for the three functions of the Aluminium EAM potential are shown below.

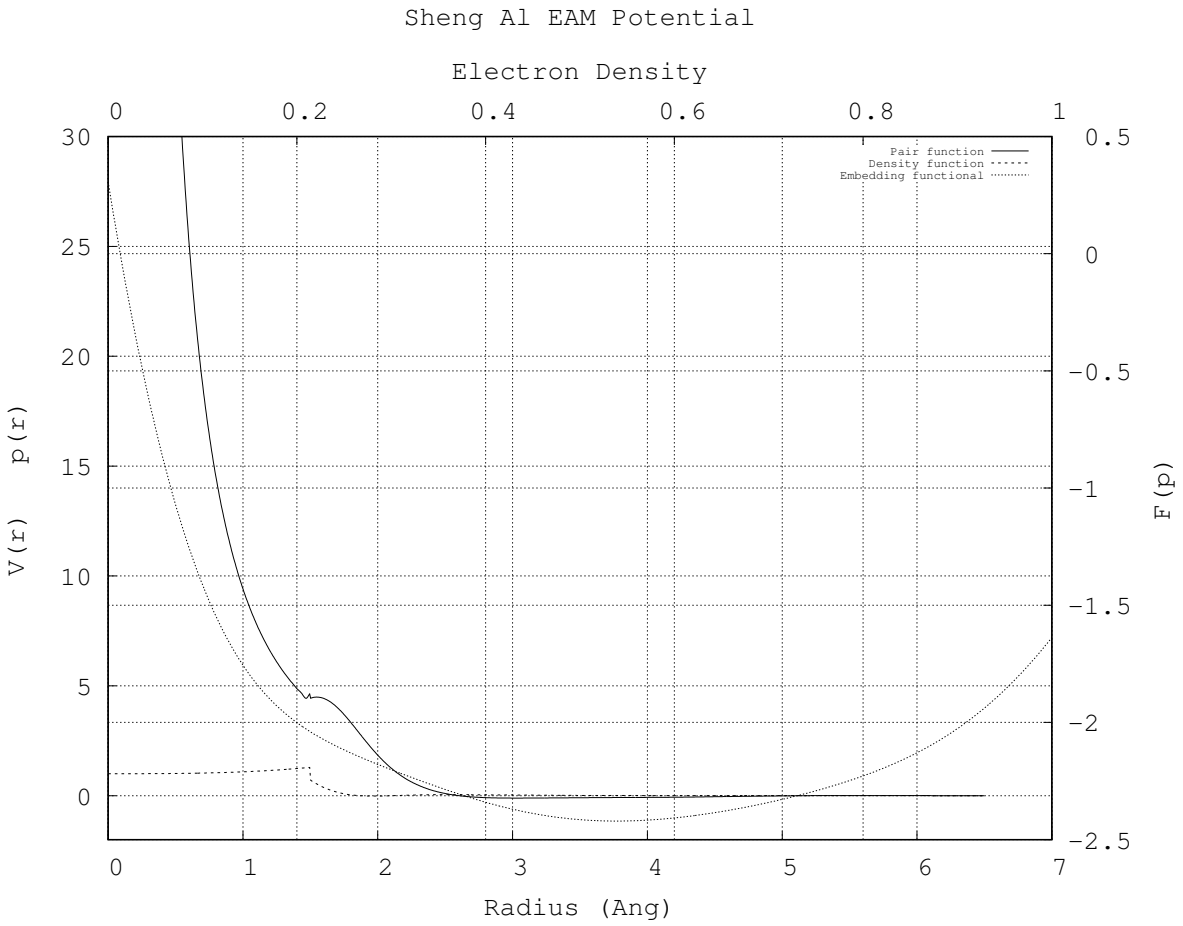


Figure 5.1: Graph caption

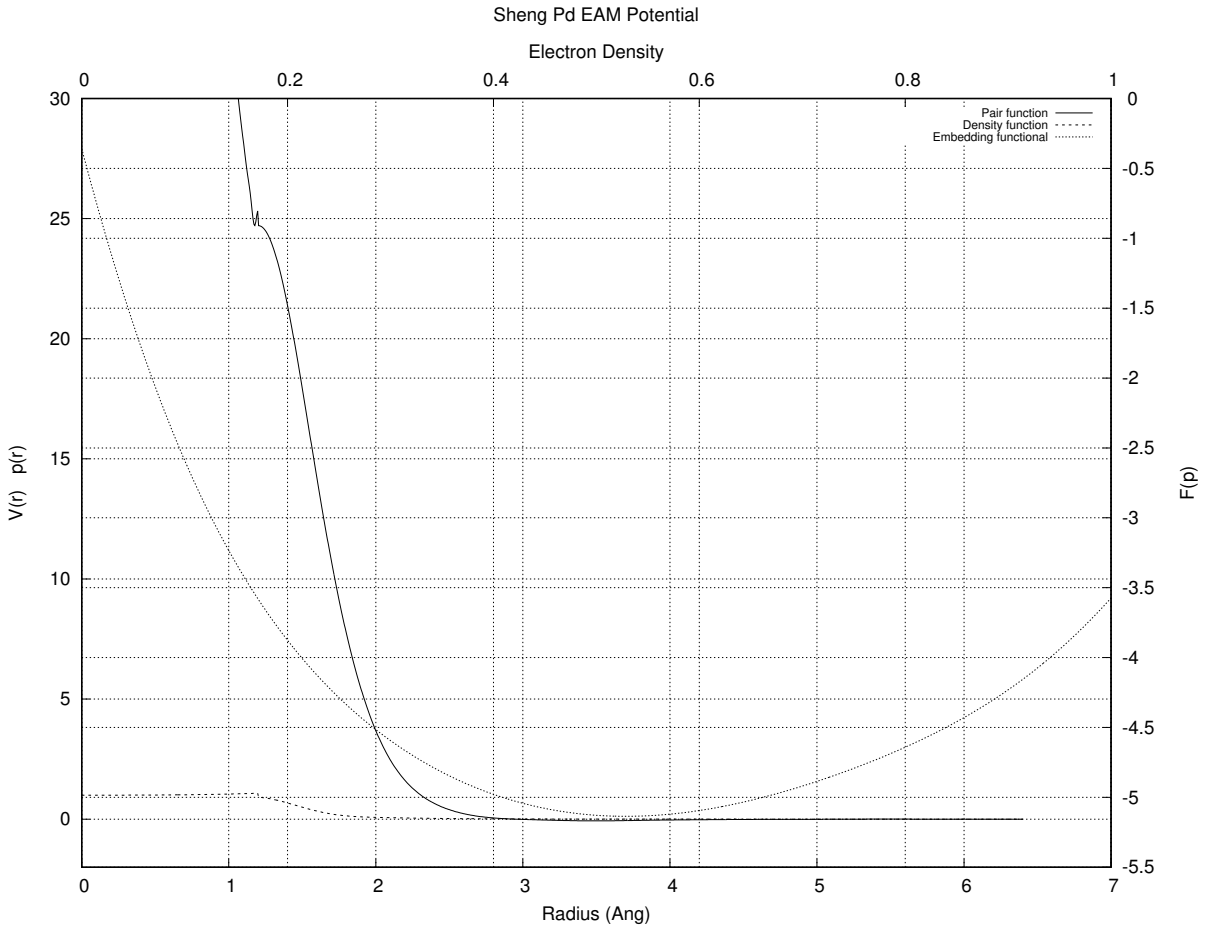


Figure 5.2: Graph caption

## Two Band Embedded Atom Method

There are several variations of the EAM potential, and one of particular interest to us is the two-band model EAM (2BMEAM) that has two electron density and embedding energy terms. This formalism was originally developed to model Caesium (14), and the transition of electrons between S and D bands under pressure, but it has been modified to apply to alloys.

An alloy version of the two-band model was developed by Olsson et al. to investigate the -prime phase formation in Fe-Cr (15). It was further developed by Bonny et al to provide a reliable EAM type potential to model high-chromium ferritic alloys (16). This potential correctly predicts the change of sign in mixing enthalpy as the local concentration of Chromium changes, and the functions take the following form.

$$\begin{aligned} U_{EAM} &= \frac{1}{2}\sum_{i=1}^{N}\sum_{j\neq i}^{N} V_{ij}(r_{ij}) + \sum_{i=1}^{N} F_D[\rho_{d,i}] + \sum_{i=1}^{N} F_S[\rho_{s,i}] \\ \text{where } \rho_{d,i} &= \sum_{j=i,j\neq i}^{N} \rho_{d,ij}(r_{ij}) \text{ and } \rho_{s,i} = \sum_{j=i,j\neq i}^{N} \rho_{s,ij}(r_{ij}) \end{aligned} \tag{5.2}$$

This allows a second embedding functional and electron density function to add/subtract energy to an atom when mixed as an alloy, but reverts to the original EAM for that element when in local concentrations of like-atoms.

2.6.4 Functional Forms of Embedded Atom Method Potentials

The functions used to represent the pair potential, electron density and embedding functional can be tabulated or calculated from analytic functions. By using an analytic function, there is the advantage of being able to produce tabulated versions of the potential functions and functional if required.

In a derivation of an EAM potential for Iron by Mendelev et al (17) the authors use a hybrid function between two exponential functions and a polynomial spline to represent the pair potential, and polynomial splines to represent the electron density function and embedding functional. Similarly, a potential has been derived for Uranium by Smirnova et al (18) that uses polynomial splines exclusively for the pair and density functions, and embedding functional.

Polynomial splines are attractive because they are continuous, have a continuous first order derivative for third order polynomials, a continuous second order derivative for fifth order polynomials, and they are flexible enough to create a potential that reproduces the forces predicted by Ab Initio. Although each segment of the spline is determined by four parameters, the nodes between splines can be adjusted which reduces the number of parameters that are adjusted during the derivation process.

Two forms of polynomial spline have been used in the literature:

$$f(r) = \sum_{i=1}^{n} A_i(r_i - r)H(r_i - r) \tag{5.3}$$

$$f(r) = \sum_{i=1}^{n} (a_i r^3 + b_i r^2 + c_i r + d_i)H(r_i^{upper} - r)H(r - r_i^{lower}) \tag{5.4}$$

The first type of spline has fewer parameters, but is a superposition of two or more polynomials up until the spline segment between the final two cutoff points. This makes it tricky to fit the parameters to give a desired starting potential. In the second type of spline, a single polynomial stitches between any two nodes. The boundary conditions at each node are: the output of the functions either side of the node be equal the first and second derivatives of the polynomials either side of the node are equal at the node While there are more

parameters to fit for the second type of spline, the number can be reduced by varying the position of the nodes and calculating the parameters by fitting the polynomials between the nodes. Given that we are deriving potentials for a metal alloy, a many body potential is needed. The EAM potential is a more general form of the Finnis-Sinclair type potential, and it has been used in many molecular dynamics investigations into metals. For these reasons, our aim is to derive EAM potentials for Fe-Pd and Fe-Ru. Two-band method EAMs have additional degrees of freedom and may be useful as they can capture any changes in the potential as the species mix and form the alloy. This is a secondary aim, the primary being standard EAM potentials. Molecular dynamics codes are capable of using tabulated functions. The form of the potential derived will be a spline of many polynomials that will be used to produce the tabulated versions of the potential functions. These are more flexible than other analytical potentials, they can be easily splined to other functions (such as the hard core Ziegler Biersack Littmark [ZBL] hard core potential) and continuous first and second derivatives can be forced. Four a fourth order polynomial spline, the functions all take the following form:

$$f(r) = \sum_{i=1}^{n} (a_i r^3 + b_i r^2 + c_i r + d_i) H(r_i^{upper} - r) H(r - r_i^{lower}) \tag{5.5}$$

# Fitting Interatomic Potentials

## Analysing a Potential

To fit a potential, it must be analysed as it is changed by comparing the behaviour of a model using this potential to experimental or DFT derived values. The properties and values being compared in this thesis are:

- total energy of a collection of atoms
- forces between a collection of atoms
- bulk modulus, optimum energy and volume for an FCC crystal structure
- $C_{11}$, $C_{12}$ and $C_{44}$ elastic constants

## Lagrange Interpolation

Lagrange interpolation is a valuable tool when evaluating or optimising potentials. Rather than fit a polynomial that exactly passes through n points, Lagrange interpolation returns the value of f(x) only. This is much faster, computationally, than fitting an nth order polynomial, but it doesn't return enough information in itself to calculate f'(x) and f"(x). By using the Lagrange interpolation algorithm recursively, the first and second derivative values are calculated. This makes it a useful tool for splining between nodes, where the x, f(x), f'(x) and f"(x) are required, and for energy and force calculations from tabulated potentials where the radius and density values of the functions/functionals fall between tabulated points. For a set of data points:

$$D = \{(x_0, y_0)\} \tag{5.6}$$

An alternative method is to set up a system of linear equations and solve this by matrix inversion. Using Fortran, both methods were evaluated for three, four and five point interpolation. The outcome is that Lagrange Interpolation shows a decrease of processing time of up to a factor of ten.

# Chapter 6

# Methodology: Proton Activation and Radioactive Decay

*Chapter Summary*

## Activation by Ion Irradiation

The Bateman equation was derived using Laplace transforms, and this same method has been used to develop a modified equation that incorporates branching factors and production rates for each isotope in the decay chain, as illustrated by Figure 6.1.

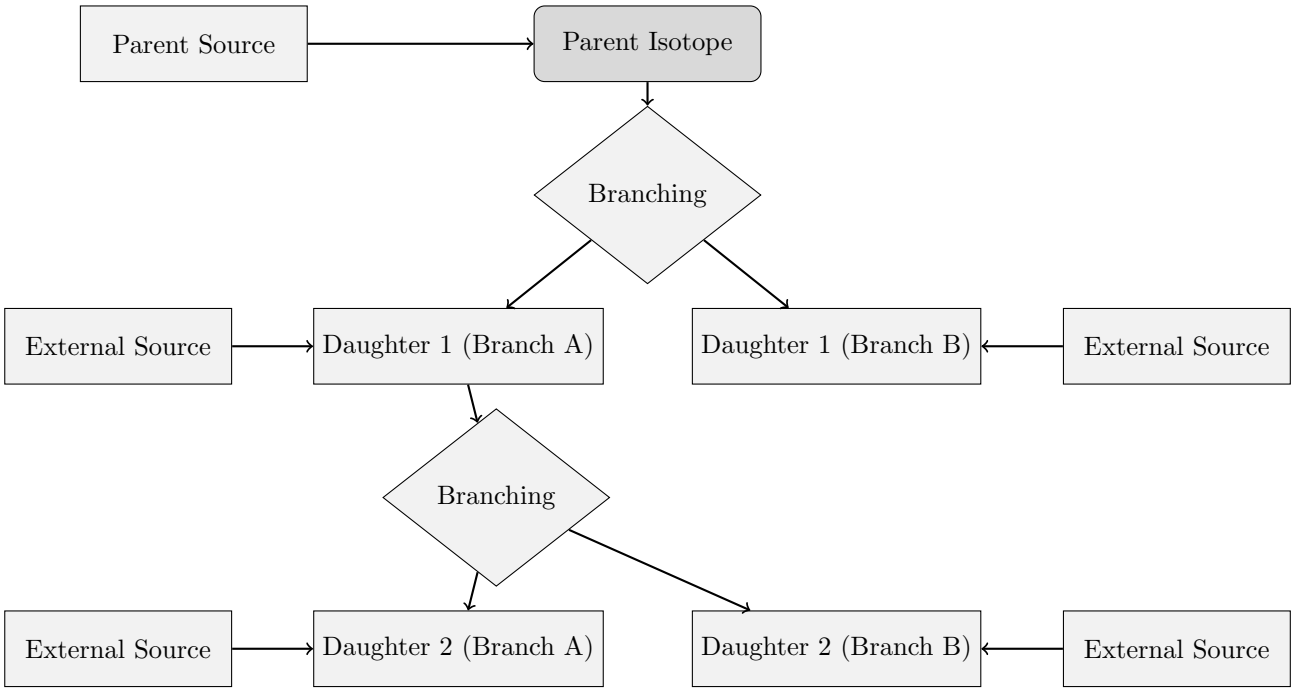


*Figure 6.1: An example of several decay chains including branching factors and possible external source terms for each isotope on each chain.*

## Laplace Transform

Laplace Transforms (6.1) are a useful mathematical tool, and allow ordinary differential equations to be solved by simple algebraic manipulation in the s domain. Bateman took advantage of Laplace Transforms in deriving his equation, and this is the method that has been taken here as well.

$$F(s) = \int_0^\infty f(t) \exp(-st) dt \tag{6.1}$$

## Constructing the Differential Equations

The first step is to set up differential equations for the parent isotope, unstable daughter isotopes and stable daughter isotope. The parent isotope has a source term, due to production, and a loss term, due to decay. The unstable daughter isotopes have two source terms, from the production by irradiation induced transmutation and the decay of preceding isotopes in the decay chain, and a loss term, due to decay. Finally, the stable daughter that finalizes the decay chain has two source terms (the same as the unstable daughters) but no loss term.

The variables (and vectors) used in these equations are defined as follows:

- $\vec{\lambda}$ vector containing isotope decay constants $\lambda_i$
- $\vec{b}$ vector containing isotope to isotope branching factors $b_i$
- $\vec{w}$ vector containing isotope production rates $w_i$
- $t$ time at which activity/amount of isotope is measured
- $N_i(0)$ starting amount of the $\mathrm{i}^{\mathrm{th}}$ isotope
- $N_i(t)$ amount of the $\mathrm{i}^{\mathrm{th}}$ isotope at time t
- $N_i'(t)$ change in amount of the $\mathrm{i}^{\mathrm{th}}$ isotope, with respect to time, at time t

The differential equations for the parent isotope (first isotope), unstable daughter isotopes ($\mathrm{i}^{\mathrm{th}}$ isotopes) and stable, final, daughter isotope (zth isotope) in the time domain are as follows:

$$N_1'(t) = \omega_1 - \lambda_1 N_1(t) \tag{6.2}$$

$$N_i'(t) = \omega_i + b_{i-1}\lambda_{i-1}N_{i-1}(t) - \lambda_i N_i(t) \tag{6.3}$$

$$N_z'(t) = \omega_z + b_{z-1}\lambda_{z-1}N_{z-1}(t) \tag{6.4}$$

Applying the Laplace Transform to these three differential equations allows them to be manipulated and solved algebraically in the s-domain.

$$N_1(s) = \frac{1}{s+\lambda_1} N_1(0) + \frac{1}{s(s+\lambda_1)} \omega_1 \tag{6.5}$$

$$N_i(s) = \frac{1}{s(s+\lambda_i)} (\omega_i) + \frac{1}{s+\lambda_i} (b_{i-1}\lambda_{i-1}N_{i-1}(s)) + \frac{1}{s+\lambda_i} N_i(0) \tag{6.6}$$

$$N_z(s) = \frac{1}{s^2}\omega_z + \frac{1}{s}b_{z-1}\lambda_{z-1}N_{z-1}(s) + \frac{1}{s}N_z(0) \tag{6.7}$$

## Numerical Inversion of the Laplace Transform

The Gaver-Stehfest[7] algorithm was developed in the 1960s and 1970s and is a method of calculating the inverse of a Laplace Transform in the real number domain. It is an easy to implement and reasonably accurate method, although it is an approximation to the real value. A comparison between an analytic and numeric inversion for the unstable isotope Po-218 is discussed at the end of this section (figure 6.2).

$$f(t) \approx f_n(t) = \frac{\ln(2)}{t}\sum_{k=1}^{2n} a_k(n)F(s) \text{ where } n \geq 1, t > 0 \tag{6.8}$$

$$s = \frac{k\ln(2)}{t} \tag{6.9}$$

$$a_k(n) = \frac{(-1)^{(n+k)}}{n!}\sum_{j=Floor(\frac{k+1}{2})} j^{n+1}\binom{n}{j}\binom{2j}{j}\binom{j}{k-j} \tag{6.10}$$

The equation for the i$^{\text{th}}$ isotope may be calculated by recursively calculating the equations by numeric inversion, starting from the first (parent isotope) and inserting the result into each subsequent recursion until the i$^{\text{th}}$ isotope is reached (changing the equations appropriately for the parent, unstable daugher and stable daughter isotopes).

## Analytic Solution by Partial Fraction Expansion

The equation for the i$^{\text{th}}$ isotope in the s domain can be written in full by substituting the preceding equation until the parent isotope is reached, and this full equation may be rearranged with the production amount of each isotope and starting amount of each isotope in individual terms. Each of these terms is multiplied by a fraction that can be expanded, using partial fractions, and inverted analytically.

This is illustrated with an example unstable isotope, fourth in the decay chain (including the parent isotope):

$$\begin{aligned}
N_4(s) = {} & \frac{1}{(s+\lambda_1)(s+\lambda_2)(s+\lambda_3)(s+\lambda_4)}b_2b_3b_4\lambda_1\lambda_2\lambda_3N_1(0) \\
& + \frac{1}{(s+\lambda_2)(s+\lambda_3)(s+\lambda_4)}b_3b_4\lambda_2\lambda_3N_2(0) \\
& + \frac{1}{(s+\lambda_3)(s+\lambda_4)}b_4\lambda_3N_3(0) \\
& + \frac{1}{(s+\lambda_4)}N_4(0) \\
& + \frac{1}{s(s+\lambda_1)(s+\lambda_2)(s+\lambda_3)(s+\lambda_4)}b_2b_3b_4\lambda_1\lambda_2\lambda_3\omega_1 \\
& + \frac{1}{s(s+\lambda_2)(s+\lambda_3)(s+\lambda_4)}b_3b_4\lambda_2\lambda_3\omega_2 \\
& + \frac{1}{s(s+\lambda_3)(s+\lambda_4)}b_4\lambda_3\omega_3 \\
& + \frac{1}{s(s+\lambda_4)}\omega_4
\end{aligned} \tag{6.11}$$

An example stable isotope, fourth (last) in the decay chain (including the parent isotope):

$$
\begin{aligned}
N_4(s) = &\frac{1}{s(s+\lambda_1)(s+\lambda_2)(s+\lambda_3)} b_2 b_3 b_4 \lambda_1 \lambda_2 \lambda_3 N_1(0) \\
&+ \frac{1}{s(s+\lambda_2)(s+\lambda_3)} b_3 b_4 \lambda_2 \lambda_3 N_2(0) \\
&+ \frac{1}{s(s+\lambda_3)} b_4 \lambda_3 N_3(0) \\
&+ N_4(0) \\
&+ \frac{1}{s^2(s+\lambda_1)(s+\lambda_2)(s+\lambda_3)} b_2 b_3 b_4 \lambda_1 \lambda_2 \lambda_3 \omega_1 \\
&+ \frac{1}{s^2(s+\lambda_2)(s+\lambda_3)} b_3 b_4 \lambda_2 \lambda_3 \omega_2 \\
&+ \frac{1}{s^2(s+\lambda_3)} b_4 \lambda_3 \omega_3 \\
&+ \frac{1}{s^2} \omega_4
\end{aligned}
\tag{6.12}
$$

By using partial fraction expansion and standard Laplace Transforms, the set of equations below is used to calculate the amount of the $\mathrm{m}^{\mathrm{th}}$ isotope in the decay chain, providing the $\mathrm{m}^{\mathrm{th}}$ isotope is unstable.

$$
N_m(t; \vec{\lambda}, \vec{b}, \vec{w}) = \sum_{k=1,m} r(k; \vec{\lambda}, \vec{b}) \left[ f(t; k, m, \vec{\lambda}) N_k(0) + g(t; k, m, \vec{\lambda}) w_k \right] \tag{6.13}
$$

$$
r(k, m, \vec{\lambda}) = \begin{cases} \prod_{i=k,m-1} \left( b_{i+1} \lambda_i \right), & \text{if } k < m \\ 1, & \text{if } k = m \end{cases} \tag{6.14}
$$

$$
f(t; k, m, \vec{\lambda}) = (-1)^{m-k} \sum_{i=k,m} \left[ \exp(-\lambda_i t) \prod_{j=k,m; j \neq i} \left( \frac{1}{\lambda_i - \lambda_j} \right) \right] \tag{6.15}
$$

$$
g(t; k, m, \vec{\lambda}) = \frac{1}{\prod_{i=k,m} \lambda_i} + (-1)^{m-k+1} \sum_{i=k,m} \left[ \frac{1}{\lambda_i} \exp(-\lambda_i t) \prod_{j=k,m; j \neq i} \left( \frac{1}{\lambda_i - \lambda_j} \right) \right] \tag{6.16}
$$

The set of equations below is used to calculate the amount of the $\mathrm{m}^{\mathrm{th}}$ isotope in the decay chain, where the $\mathrm{m}^{\mathrm{th}}$ isotope is stable.

$$
N_m(t; \vec{\lambda}, \vec{b}, \vec{w}) = N_m + w_m t + \sum_{k=1,m-1} r(k; \vec{\lambda}, \vec{b}) \left[ f(t; k, m-1, \vec{\lambda}) N_k(0) + g(t; k, m, \vec{\lambda}) w_k \right] \tag{6.17}
$$

$$
r(k, m, \vec{\lambda}) = \begin{cases} \prod_{i=k,m-1} \left( b_{i+1} \lambda_i \right), & \text{if } k < m \\ 1, & \text{if } k = m \end{cases} \tag{6.18}
$$

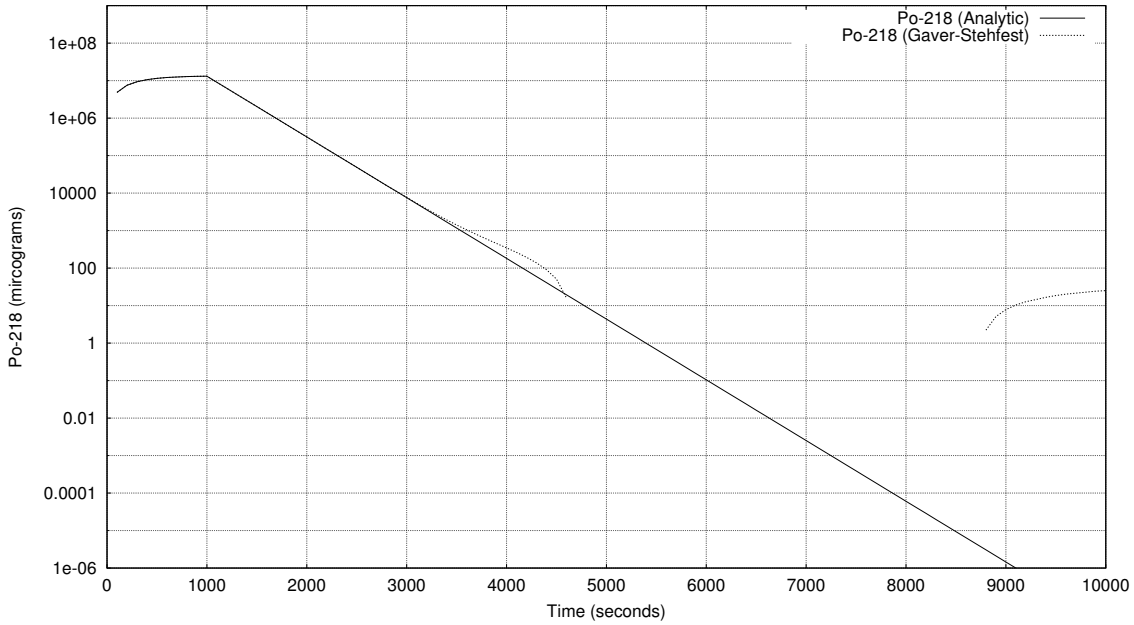


*Figure 6.2: Decay of Po-218: Analytice and Gaver-Stehfest Calculations [6]*

$$f(t;k,m,\vec{\lambda}) = \frac{1}{\prod_{i=k,m}\lambda_i} + (-1)^{m-k+1}\sum_{i=k,m}\left[\frac{1}{\lambda_i}\exp(-\lambda_i t)\prod_{j=k,m;j\neq i}\left(\frac{1}{\lambda_i-\lambda_j}\right)\right] \tag{6.19}$$

$$g(t;k,m,\vec{\lambda}) = \frac{1}{\prod_{i=k,m}\lambda_i}t + \frac{\sum_{i=k,m}\left[\prod_{j=k,m;j\neq i}\lambda_j\right]}{\prod_{i=k,m}\lambda_i^2} + (-1)^{m-k+1}\sum_{i=k,m}\left[\frac{1}{\lambda_i^2}\exp(-\lambda_i t)\prod_{j=k,m;j\neq i}\left(\frac{1}{\lambda_i-\lambda_j}\right)\right] \tag{6.20}$$

### Preference: Analytic over Numeric

The numeric solution only requires the equation to be solved in the s-domain; the Gaver-Stehfest algorithm performs the inversion. It is worth the extra effort to derive and implement an analytic solution, as the numeric is only an approximation. Examples of the pitfalls of the numeric solution are that it can give negative amounts of an isotope and the difference between the numeric and analytic calculated amounts can become quite large when the isotope decays away to a very small value. Figure 6.2 shows the predicted decay of a sample of Po-218 irradiated for 1,000s, and sampled until 10,000s. In the region between 4,000s and 9,000s the amount from the numeric calculation drops below zero, whereas the analytic calculation remains above zero, as would be expected.

## Computational Methods

The Activity program has been developed in Fortran and takes advantage of MPI (Message Parsing Interface) to speed up calculation times by allowing the use of multiple processes in parallel. It has a self contained maths library, although this could be improved in the future by using optimised maths libraries for certain functions (e.g. matrix operations).

The code was developed on a Debian based distribution of Linux, but it should be supported on other variants of Linux and Unix, and does not require any specialist hardware.

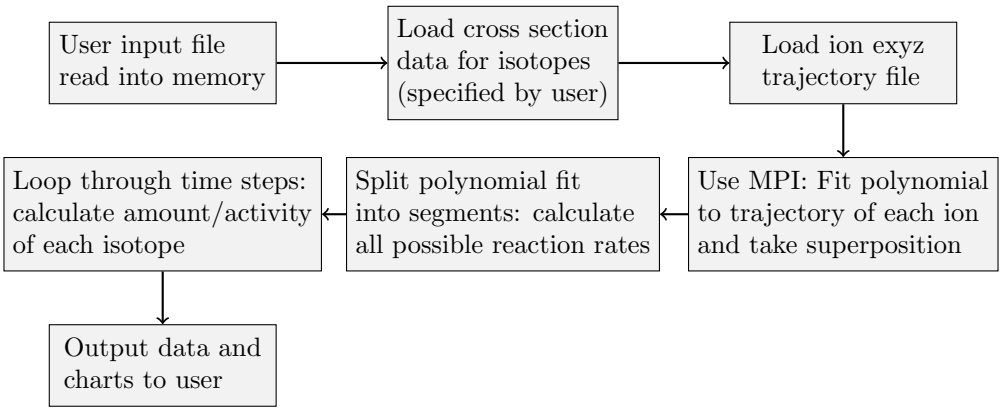


*Figure 6.3: Flow chart of major processes in the Activity code*

The user is required to prepare an input file that contains the instructions required to perform a calculation. In addition to the input file, the user must provide an EXYZ ion trajectory file output by SRIM. Activity will read in the user input file, and the SRIM and data files listed within, before performing the calculation. Figure 6.3 shows a flowchart of the major steps the code performs.

There are various settings in the user input file, but the main ones relating to the simulated experiment are:

- Element composition of target (percentage by mass).
- Beam flux (current), energy, duration and area on target.
- Activity measurement time (end of the "experiment").
- Material density.
- Target thickness.

# Chapter 7

# Methodology: Interatomic Potential Fitting

*Chapter Summary*

## High Performance Computing

Brief: throughout the process, DFT, potential fitting and future kmc or MD simulations, need high performance computing. Time applied for on Archer and BlueBEAR.

## Interatomic Potential Fitting

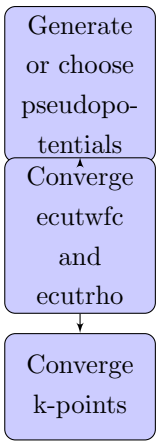


¡Intro¿

### Reference Database

In order to fit the potentials, it was necessary to build a reference database. This consists of known experimental bulk properties along with forces, energies and stresses calculated using DFT.

32 atom randomised

108 atom defects

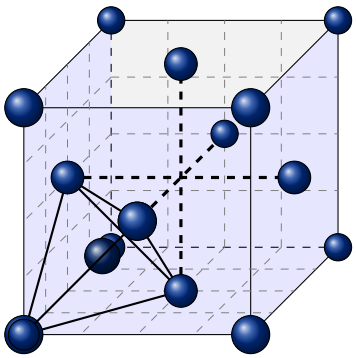

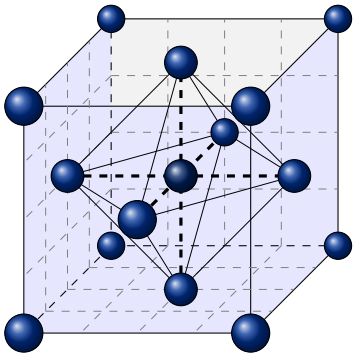

### DFT Calibration

#### Choice of Pseudopotentials

#### Energy and Charge Density Cutoffs

#### K-Points

#### nbnd

### Atomic Configurations for DFT Calculations

The interatomic potentials are designed to reproduce the forces, energies, stresses and bulk properties

## Mathematical Tools

In writing the Activity computer code and EAMPA computer code, I created a shared library of maths functions and subroutines used by either or both of the codes.

## DFT Calculations

### Pseudopotential Generation

## Potential Analysing Code

# Chapter 8

# Activity Code Development & Publication

*Chapter Summary*

## Activation by Ion Irradiation

## Computer Package Development

¡Intro¿

# Chapter 9

# Ab Initio Reference Database

*Chapter Summary*

## Activation by Ion Irradiation

## Computer Package Development

¡Intro¿

# Chapter 10

# Interatomic Potential Fitting

*Chapter Summary*

## Activation by Ion Irradiation

## Computer Package Development

Fitting a potential requires many repeated calculations of the forces and total energy of configurations of hundreds of atoms using the potential as it is varied. This puts a high demand on memory and central processing unit of a computer. Python is an easy to use high-level programming language that supports object orientated programming. Unfortunately, parallel programming using threading is hampered in Python by the global interpreter lock, and by it's very nature as an interpreted language, it is much slower than a compiled language.

There are several tools available to unlock the full potential of a modern multicore processor while writing in Python.

### Cython

### F2PY

### OpenMP

### Development

The resulting was developed using python and a shared object library written in Fortran 90 and compiled using F2PY.

# Chapter 11

# Molecular Dynamics

*Chapter Summary*

## Activation by Ion Irradiation

## Computer Package Development

¡Intro¿

# Chapter 12

# Conclusions

*Chapter Summary*

¡Intro¿

## Restating Objectives

### Contributions of this Thesis While Answering the Original Question

# Chapter 13

# Future Work

*Chapter Summary*

¡Intro¿

# Appendices

# Appendix A

# DFT Calibration

Table A.1: Nbnd settings

| | Al | Cr | Fe | Ru | Pd |
|---|---|---|---|---|---|
| Valence Electrons | 3 | 14 | 16 | 16 | 18 |
| Nbnd 1 atom | 3 | 10 | 12 | 12 | 13 |
| Nbnd 2 atoms | 5 | 20 | 23 | 23 | 26 |
| Nbnd 4 atoms | 9 | 40 | 45 | 45 | 51 |
| Nbnd 16 atoms | 34 | 157 | 180 | 180 | 202 |
| Nbnd 31 atoms | 66 | 304 | 348 | 348 | 391 |
| Nbnd 32 atoms | 68 | 314 | 359 | 359 | 404 |
| Nbnd 33 atoms | 70 | 324 | 370 | 370 | 416 |
| Nbnd 107 atoms | 225 | 1049 | 1199 | 1199 | 1349 |
| Nbnd 108 atoms | 227 | 1059 | 1210 | 1210 | 1361 |
| Nbnd 109 atoms | 229 | 1069 | 1221 | 1221 | 1374 |
| Nbnd 255 atoms | 536 | 2499 | 2856 | 2856 | 3213 |
| Nbnd 256 atoms | 538 | 2509 | 2868 | 2868 | 3226 |
| Nbnd 257 atoms | 540 | 2519 | 2879 | 2879 | 3239 |

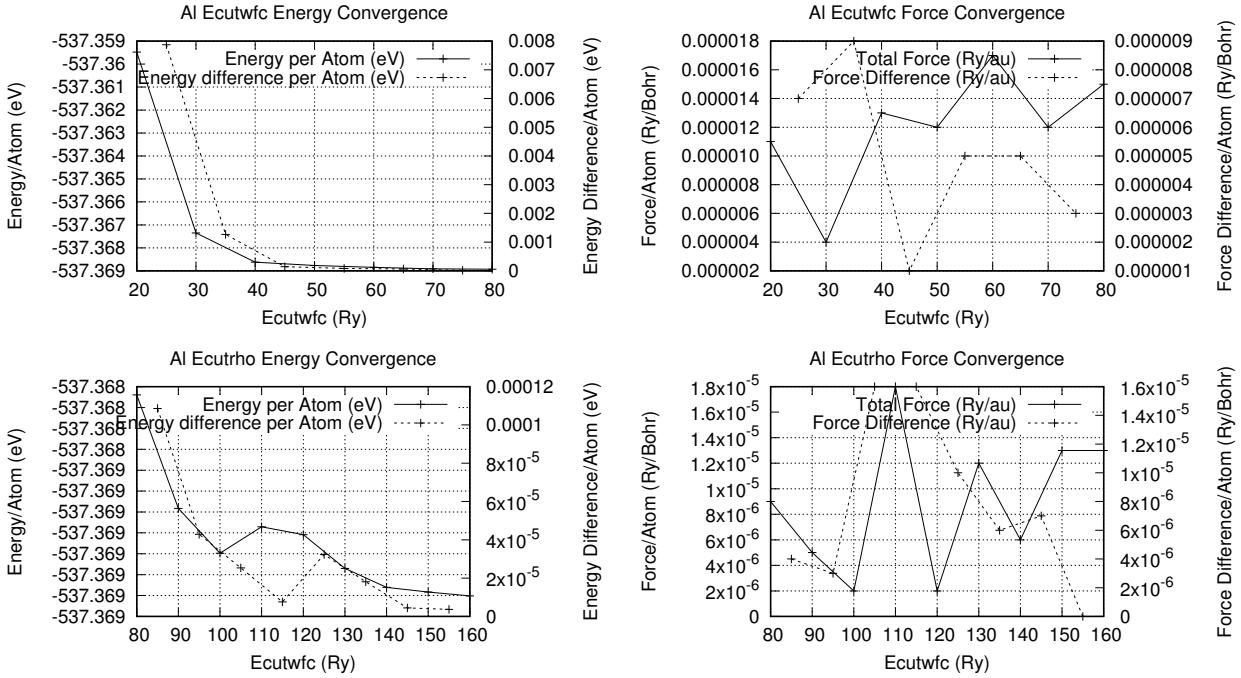


Figure A.1: Graph caption

# Ecutwfc and Ecutrho Convergence

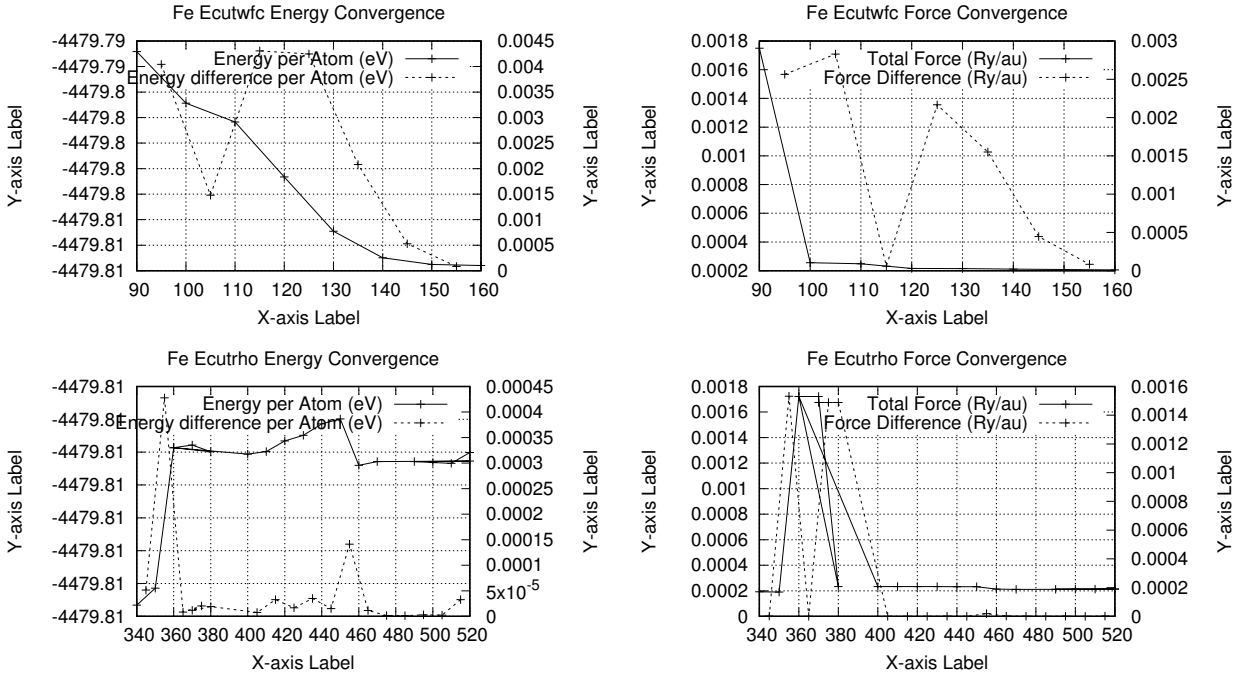


Figure A.2: Graph caption

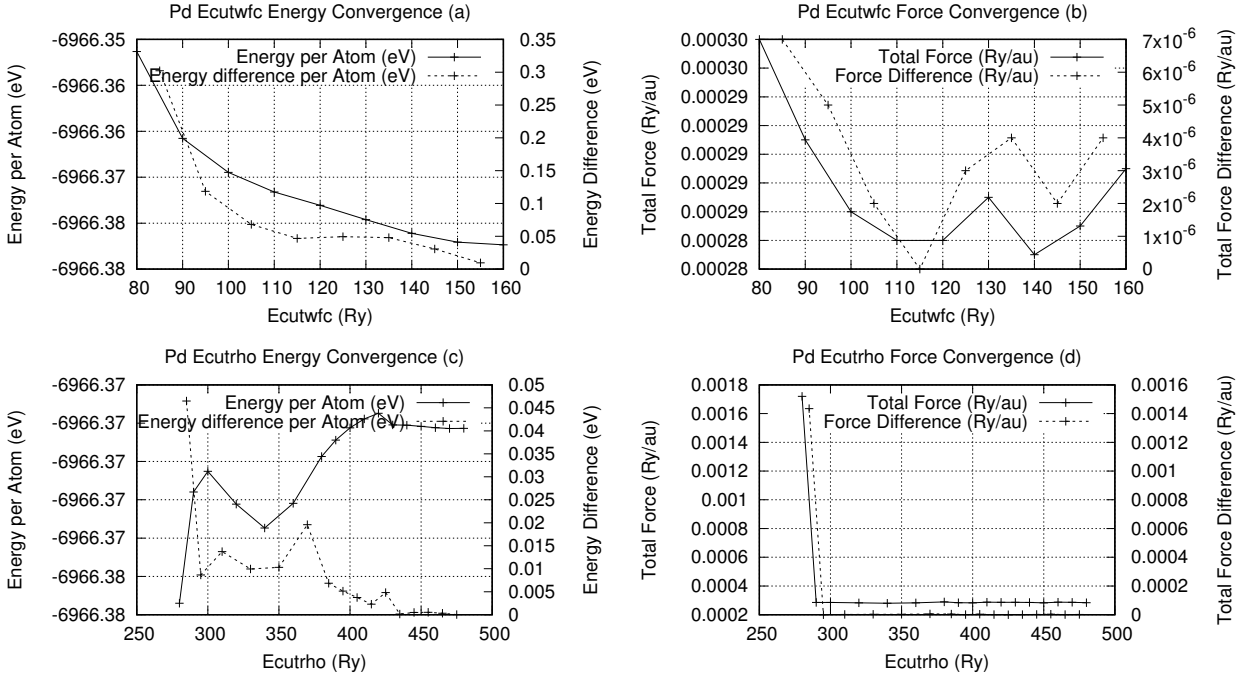


Figure A.3: Graph caption

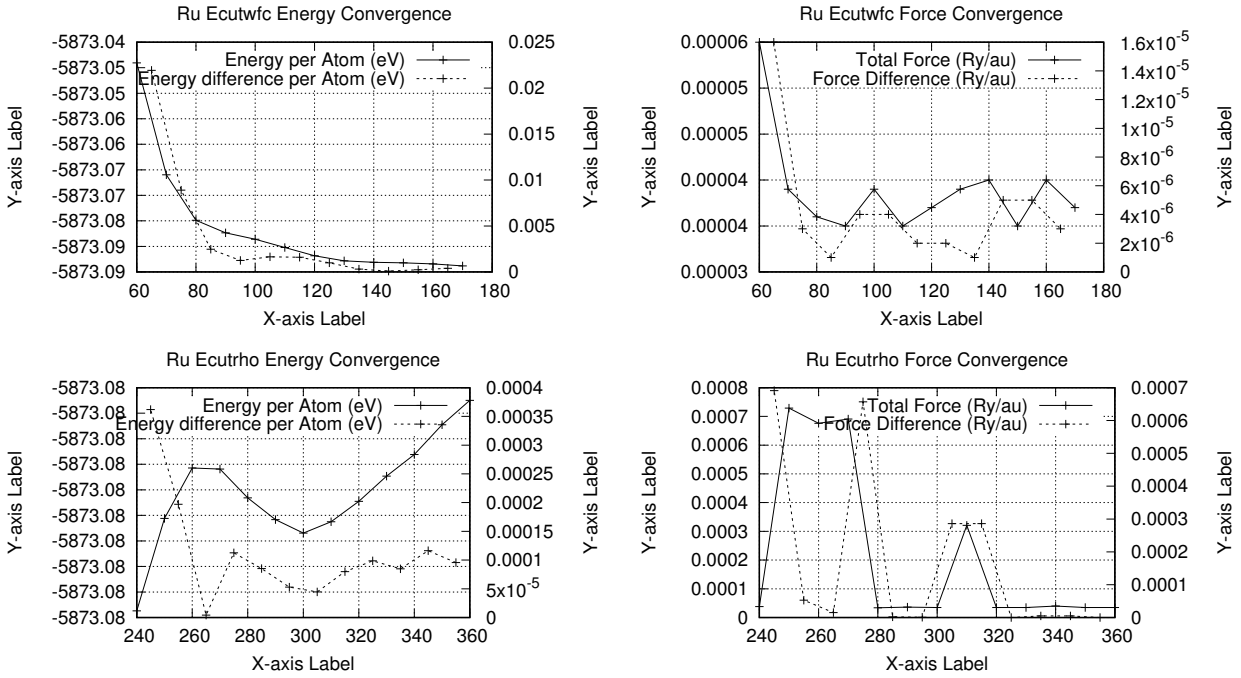


Figure A.4: Graph caption

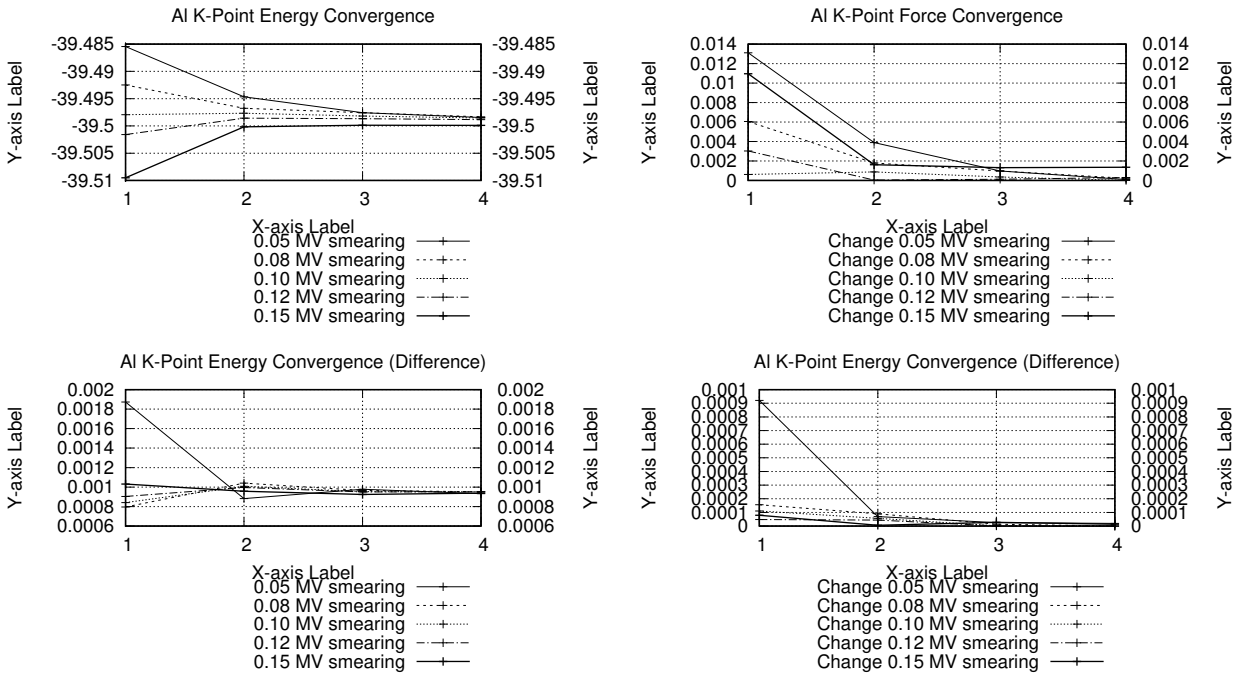


Figure A.5: Graph caption

# K-point Convergence

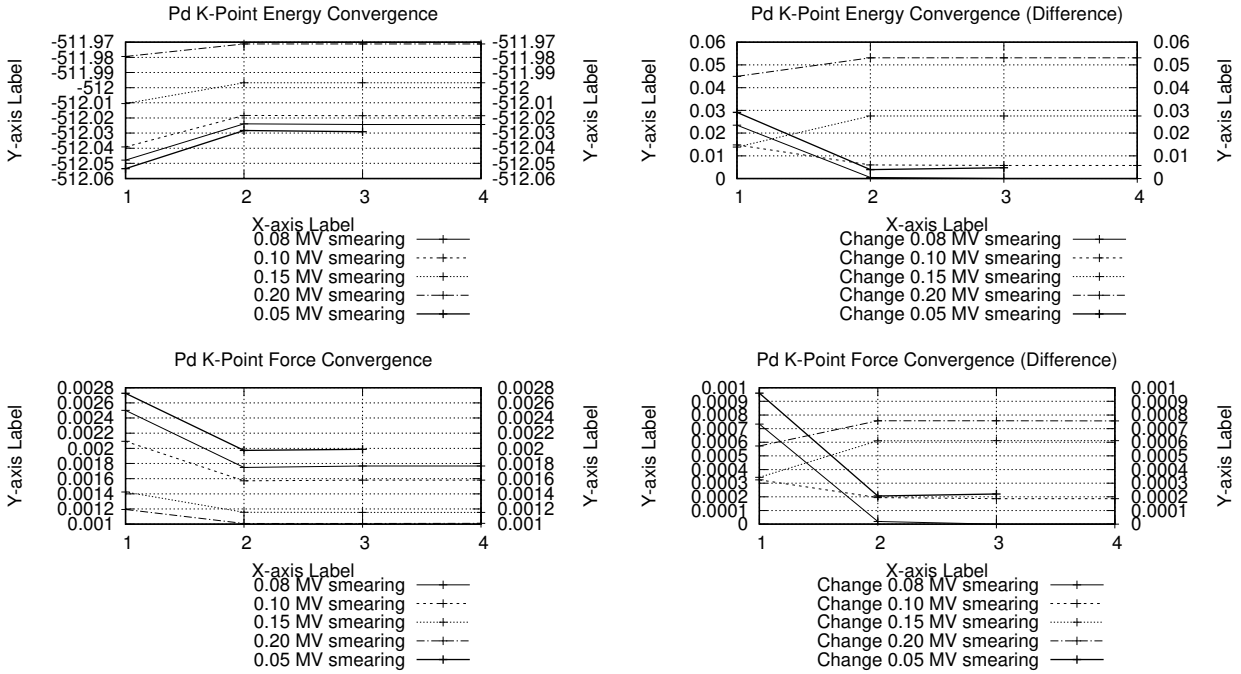


Figure A.6: Graph caption

# Appendix B

# Important Codes and Scripts

The contents...

# Appendix C

# Activity Paper published in Computer Physics Communications

Computer Physics Communications 216 (2017) 138–144

Contents lists available at ScienceDirect

Computer Physics Communications

journal homepage: www.elsevier.com/locate/cpc

# Activity computer program for calculating ion irradiation activation☆

Ben Palmer *, Brian Connolly, Mark Read

*University of Birmingham, United Kingdom*

ARTICLE INFO

*Article history:*
Received 1 June 2015
Received in revised form 15 February 2017
Accepted 19 February 2017
Available online 29 March 2017

ABSTRACT

A computer program, Activity, was developed to predict the activity and gamma lines of materials irradiated with an ion beam. It uses the TENDL (Koning and Rochman, 2012) [1] proton reaction cross section database, the Stopping and Range of Ions in Matter (SRIM) (Biersack et al., 2010) code, a Nuclear Data Services (NDS) radioactive decay database (Sonzogni, 2006) [2] and an ENDF gamma decay database (Herman and Chadwick, 2006) [3]. An extended version of Bateman's equation is used to calculate the activity at time t, and this equation is solved analytically, with the option to also solve by numeric inverse Laplace Transform as a failsafe. The program outputs the expected activity and gamma lines of the activated material.

**Program summary**
*Program title:* Activity
*Catalogue identifier:* AFBS_v1_0
*Program summary URL:* http://cpc.cs.qub.ac.uk/summaries/AFBS_v1_0.html
*Program obtainable from:* CPC Program Library, Queen's University, Belfast, N. Ireland
*Licensing provisions:* GNU GPL v3
*No. of lines in distributed program, including test data, etc.:* 688828
*No. of bytes in distributed program, including test data, etc.:* 71056048
*Distribution format:* tar.gz
*Programming language:* Fortran.
*Computer:* PCs or HPCs.
*Operating system:* Linux (tested on Debian).
*Has the code been vectorized or parallelized?:* OpenMPI
*RAM:* 250MB per process + 200MB overhead
*Classification:* 2.2, 17.8.

*Nature of problem:* To calculate the predicted activity of an ion irradiated target. The expected range of ion energies is between 1MeV and 200MeV; this is the range of the available ion cross section data.

*Solution method:* The program loads cross section data from the TENDL database and trajectory data from a SRIM [1] simulation exyz data file. It uses this data to calculate the production/loss rate of each isotope in the simulated target. Radioactive decay equations are used to calculate the amounts and activity of each radioactive isotope at the set time.

*Running time:* Typically the Activity program runs each input from seconds to no more than several minutes.

*References:*

[1] SRIM — The stopping and range of ions in matter (2010). Ziegler, James F., Ziegler, M.D. and Biersack, J.P. 2010, Nuclear Instruments and Methods in Physics Research Section B, Vol. 268, pp. 1818–1823.



☆ This paper and its associated computer program are available via the Computer Physics Communication homepage on ScienceDirect (http://www.sciencedirect.com/science/journal/00104655).

* Corresponding author.
*E-mail address:* benpalmer1983@gmail.com (B. Palmer).

http://dx.doi.org/10.1016/j.cpc.2017.02.025
0010-4655/

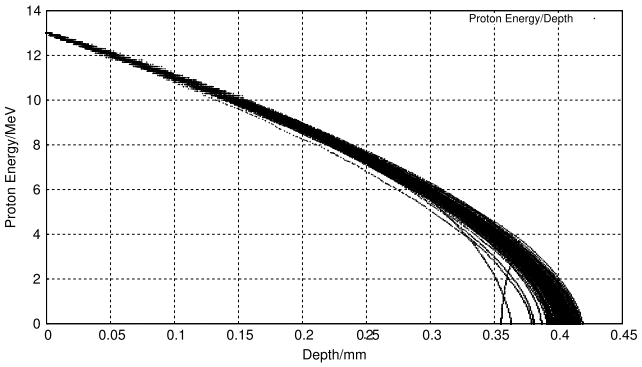


**Fig. 1.** One hundred simulated 13 MeV proton energy loss curves in Fe simulated with SRIM [4].

## 1. Background

### 1.1. Ion irradiation at the University of Birmingham

The Scanditronix MC-40 Cyclotron is used at the University of Birmingham to create a beam of protons or other light ions. The energies of these ions are typically between 10 MeV and 60 MeV with beam currents ranging up to 50 μA ($3.1 \times 10^{14}$ protons per second). Target materials are irradiated by this cyclotron for a number of reasons, including purposely creating radioactive isotopes for the nearby Queen Elizabeth Hospital, investigating ion irradiation damage and emulating neutron irradiation.

The cyclotron is usually used to create radioactive isotopes for medical use, but an additional beam line has been devoted to material science investigations into radiation damage. While the creation of radioactive isotopes is desired in some cases, material being tested for radiation damage should preferably have low levels of radioactivity.

It is expensive to arrange the irradiation of target materials by high energy neutrons sources, whereas it is relatively inexpensive to irradiate using an ion beam on the MC-40 Cyclotron. The energies can be controlled, and a set dose at a single energy, or a range of energies, can be precisely deposited into the target material.

The Activity code discussed here was developed to calculate the activity of a target material irradiated by a proton beam. It has been developed in Fortran and uses data from the TENDL-2013 proton cross section database, SRIM ion transport code and NDS radioactive decay database.

### 1.2. Simulating ion irradiation with SRIM

A package of ion transport codes, SRIM, is freely available to download and use to investigate the transport of ions through matter. SRIM uses the binary collision approximation (BCA) to simulate the passage of ions in a material. It is an approximate method, and one key restriction is that it does not take into account the structure of the material, and this approximation is therefore also imposed on the Activity code.

One file that SRIM creates is of importance to the Activity code, and that is the trajectory file that contains the energy and $x, y, z$ co-ordinate data points for simulated ions moving through matter. Fig. 1 shows the trajectory of one hundred 13 MeV protons entering and passing through an Iron target, and it is this set of data points (together with the cross section database) that the Activity code uses to calculate the reaction rates for the transmutation of nuclei in the target. At higher energies, the ions slow as they lose energy due to electronic stopping, but as the ion energy drops the mechanism of loss through nuclear collisions becomes important. The spreading of ion depths at lower energies is a result of the higher momentum transfer during nuclear collisions, as can be seen in Fig. 1.

### 1.3. Transmutation of nuclei by ion irradiation

Considering a simplified nuclear potential well, energetic protons approaching a nucleus may overcome the Coulomb potential barrier. They are captured by the nucleus and held within the potential well by the strong nuclear force. This process may leave the nucleus in an excited and unstable state, depending on the input energy of the proton and configuration of nucleons. The process is probabilistic, and the average chance of a reaction (the microscopic cross section) may be measured as a function of the projectile, projectile energy and target, either experimentally or by optical model potential calculations. The reaction rate is calculated from the microscopic cross section using the following equation:

$$R = \frac{J}{e} n_t \sigma \cdot 10^{-28} \delta t \tag{1}$$

- R Reaction Rate (reactions per second)
- J Beam current (A)
- $n_t$ Number density of target (atoms per cubic meter)
- $\sigma$ Microscopic reaction cross section (barns)
- e Elementary charge (1.602177E-19C)
- $\delta$T Target thickness (m).

### 1.4. Radioactive decay

Radioactive decay is the random change in nucleons or energy state of an unstable nucleus. It is impossible to predict when a single nucleus will decay, but the decay of a collection of nuclei is statistical in nature. The radioactivity and number of unstable nuclei at time $t$ can be predicted using the decay constant, $\lambda$, for the radioactive isotope. This constant is defined as follows:

$$\lambda = -\frac{N'(t)}{N(t)}. \tag{2}$$

The number of radioactive nuclei $N(t)$ at time $t$ is given by the following equation, where $N(0)$ is the starting number of nuclei:

$$N(t) = N(0) \exp(-t\lambda). \tag{3}$$

The activity $A(t)$ of the radioactive nuclei is predicted at time $t$ by using the following equations, where $N'(t)$ is the change in amount of nuclei with respect to time:

$$A(t) = -N'(t) = \lambda N(t) \tag{4}$$

$$A(t) = \lambda N(0) \exp(-t\lambda). \tag{5}$$

### 1.5. Bateman equation for radioactive decay

The English mathematician Harry Bateman derived an Eq. (6) to calculate the amount of each isotope in a decay chain, illustrated in Fig. 2, at time $t$.

$$N_n(t) = \sum_{i=1}^{i=n} \left( \left( \prod_{j=i}^{j=n-1} \lambda_{(ij+1)} \right) \sum_{j=i}^{j=n} \left( \frac{N_{i0} \exp(-\lambda_j t)}{\prod_{p=i, p\neq j}^{p=n} (\lambda_p - \lambda_j)} \right) \right). \tag{6}$$

When a radioactive isotope decays, there may be more than one mode of decay, and this leads to branching factors. Pb-214 only decays via beta decay to Bi-214, giving a branching factor of 1.0, whereas Bi-214 has a 99.979% chance of decaying to Po-214 by beta decay and a 0.021% of emitting an alpha particle and decaying to Tl-210 (branching factors of 0.99979 and 0.00021 respectively) [5].

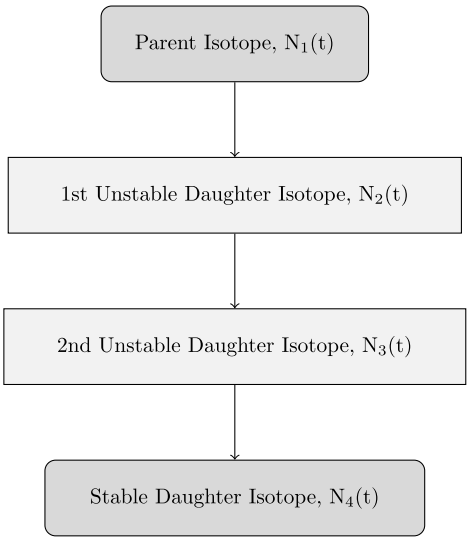


**Fig. 2.** An example decay chain from an unstable parent isotope, through unstable daughter isotopes ending with a stable daughter isotope.

When a target material is irradiated, there is a source term for transmuted nuclei due to the irradiation. The daughter isotopes of these transmuted isotopes will also be affected by the irradiation and will transmute further, giving a source term for each daughter isotope as a result of the irradiation. Sources for each isotope in the decay chain, and branching factors between a parent isotope and its daughter isotope/s must be accounted for.

The Bateman equation was derived using Laplace transforms, and this same method has been used to develop a modified equation that incorporates branching factors and production rates for each isotope in the decay chain, as illustrated by Fig. 3.

### 1.6. Laplace transform

Laplace Transforms (7) are a useful mathematical tool, and allow ordinary differential equations to be solved by simple algebraic manipulation in the s domain. Bateman took advantage of Laplace Transforms in deriving his equation, and this is the method that has been taken here as well.

$$F(s) = \int_0^\infty f(t)\exp(-st)dt. \tag{7}$$

### 1.7. Constructing the differential equations

The first step is to set up differential equations for the parent isotope, unstable daughter isotopes and stable daughter isotope. The parent isotope has a source term, due to production, and a loss term, due to decay. The unstable daughter isotopes have two source terms, from the production by irradiation induced transmutation and the decay of preceding isotopes in the decay chain, and a loss term, due to decay. Finally, the stable daughter that finalizes the decay chain has two source terms (the same as the unstable daughters) but no loss term.

The variables (and vectors) used in these equations are defined as follows:

- $\vec{\lambda}$ vector containing isotope decay constants $\lambda_i$
- $\vec{b}$ vector containing isotope to isotope branching factors $b_i$
- $\vec{w}$ vector containing isotope production rates $w_i$
- $t$ time at which activity/amount of isotope is measured
- $N_i(0)$ starting amount of the $i$th isotope
- $N_i(t)$ amount of the $i$th isotope at time $t$
- $N_i'(t)$ change in amount of the $i$th isotope, with respect to time, at time $t$.

The differential equations for the parent isotope (first isotope), unstable daughter isotopes ($i$th isotopes) and stable, final, daughter isotope ($z$th isotope) in the time domain are as follows:

$$N_1'(t) = \omega_1 - \lambda_1 N_1(t) \tag{8}$$

$$N_i'(t) = \omega_i + b_{i-1}\lambda_{i-1}N_{i-1}(t) - \lambda_i N_i(t) \tag{9}$$

$$N_z'(t) = \omega_z + b_{z-1}\lambda_{z-1}N_{z-1}(t). \tag{10}$$

Applying the Laplace Transform to these three differential equations allows them to be manipulated and solved algebraically in the s-domain.

$$N_1(s) = \frac{1}{s+\lambda_1}N_1(0) + \frac{1}{s(s+\lambda_1)}\omega_1 \tag{11}$$

$$N_i(s) = \frac{1}{s(s+\lambda_i)}(\omega_i) + \frac{1}{s+\lambda_i}(b_{i-1}\lambda_{i-1}N_{i-1}(s)) + \frac{1}{s+\lambda_i}N_i(0) \tag{12}$$

$$N_z(s) = \frac{1}{s^2}\omega_z + \frac{1}{s}b_{z-1}\lambda_{z-1}N_{z-1}(s) + \frac{1}{s}N_z(0). \tag{13}$$

### 1.8. Numerical inversion of the Laplace Transform

The Gaver–Stehfest [6] algorithm was developed in the 1960s and 1970s and is a method of calculating the inverse of a Laplace Transform in the real number domain. It is an easy to implement and reasonably accurate method, although it is an approximation to the real value. A comparison between an analytic and numeric inversion for the unstable isotope Po-218 is discussed at the end of this section (Fig. 4).

$$f(t) \approx f_n(t) = \frac{\ln(2)}{t}\sum_{k=1}^{2n} a_k(n)F(s) \text{ where } n \geq 1,\ t > 0 \tag{14}$$

$$s = \frac{k\ln(2)}{t} \tag{15}$$

$$a_k(n) = \frac{(-1)^{(n+k)}}{n!}\sum_{j=Floor(\frac{k+1}{2})} j^{n+1}\binom{n}{j}\binom{2j}{j}\binom{j}{k-j}. \tag{16}$$

The equation for the $i$th isotope may be calculated by recursively calculating the equations by numeric inversion, starting from the first (parent isotope) and inserting the result into each subsequent recursion until the $i$th isotope is reached (changing the equations appropriately for the parent, unstable daughter and stable daughter isotopes).

### 1.9. Analytic solution by partial fraction expansion

The equation for the $i$th isotope in the s domain can be written in full by substituting the preceding equation until the parent isotope is reached, and this full equation may be rearranged with the production amount of each isotope and starting amount of each isotope in individual terms. Each of these terms is multiplied by a fraction that can be expanded, using partial fractions, and inverted analytically.

This is illustrated with an example unstable isotope, fourth in the decay chain (including the parent isotope):

$$N_4(s) = \frac{1}{(s+\lambda_1)(s+\lambda_2)(s+\lambda_3)(s+\lambda_4)}b_2b_3b_4\lambda_1\lambda_2\lambda_3N_1(0)$$

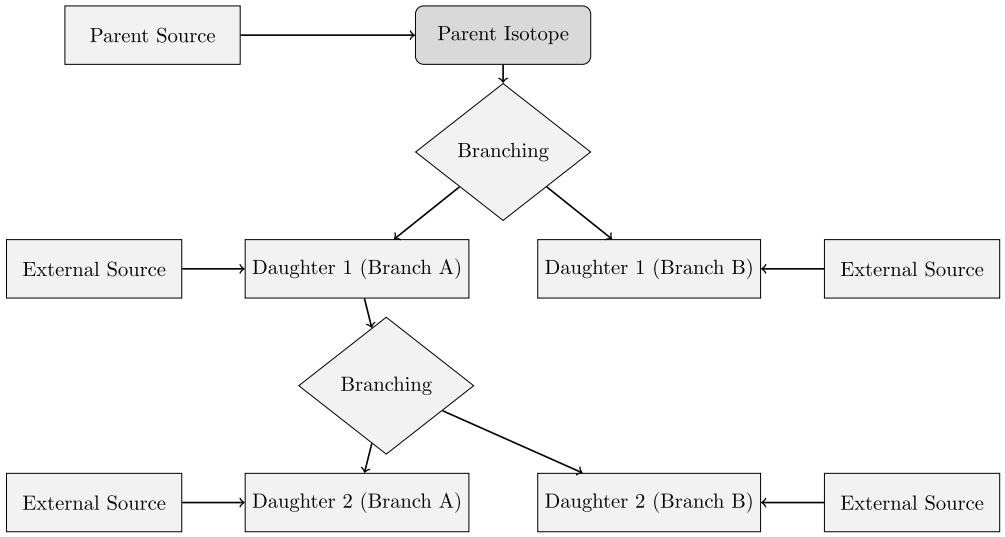


**Fig. 3.** An example of several decay chains including branching factors and possible external source terms for each isotope on each chain.

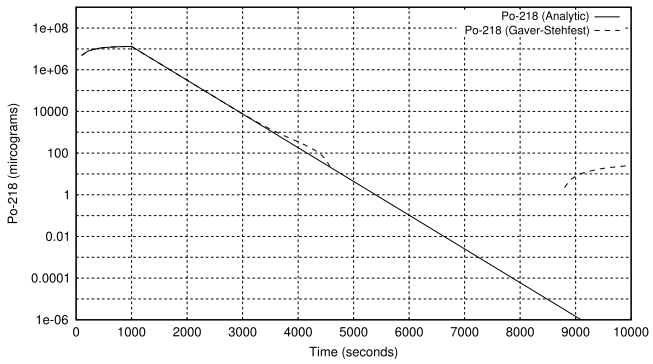


**Fig. 4.** Decay of Po-218: Analytic and Gaver– Stehfest Calculation [5].

$$
\begin{aligned}
&+\frac{1}{(s+\lambda_2)(s+\lambda_3)(s+\lambda_4)}b_3b_4\lambda_2\lambda_3N_2(0)\\
&+\frac{1}{(s+\lambda_3)(s+\lambda_4)}b_4\lambda_3N_3(0)+\frac{1}{(s+\lambda_4)}N_4(0)\\
&+\frac{1}{s(s+\lambda_1)(s+\lambda_2)(s+\lambda_3)(s+\lambda_4)}b_2b_3b_4\lambda_1\lambda_2\lambda_3\omega_1\\
&+\frac{1}{s(s+\lambda_2)(s+\lambda_3)(s+\lambda_4)}b_3b_4\lambda_2\lambda_3\omega_2\\
&+\frac{1}{s(s+\lambda_3)(s+\lambda_4)}b_4\lambda_3\omega_3+\frac{1}{s(s+\lambda_4)}\omega_4. \qquad (17)
\end{aligned}
$$

An example stable isotope, fourth (last) in the decay chain (including the parent isotope):

$$
\begin{aligned}
N_4(s) = &\frac{1}{s(s+\lambda_1)(s+\lambda_2)(s+\lambda_3)}b_2b_3b_4\lambda_1\lambda_2\lambda_3N_1(0)\\
&+\frac{1}{s(s+\lambda_2)(s+\lambda_3)}b_3b_4\lambda_2\lambda_3N_2(0)\\
&+\frac{1}{s(s+\lambda_3)}b_4\lambda_3N_3(0)+N_4(0)\\
&+\frac{1}{s^2(s+\lambda_1)(s+\lambda_2)(s+\lambda_3)}b_2b_3b_4\lambda_1\lambda_2\lambda_3\omega_1\\
&+\frac{1}{s^2(s+\lambda_2)(s+\lambda_3)}b_3b_4\lambda_2\lambda_3\omega_2\\
&+\frac{1}{s^2(s+\lambda_3)}b_4\lambda_3\omega_3+\frac{1}{s^2}\omega_4. \qquad (18)
\end{aligned}
$$

By using partial fraction expansion and standard Laplace Transforms, the set of equations below is used to calculate the amount of the $m$th isotope in the decay chain, providing the $m$th isotope is unstable.

$$
\begin{aligned}
&N_m(t;\vec{\lambda},\vec{b},\vec{w})\\
&\quad=\sum_{k=1,m}r(k;\vec{\lambda},\vec{b})\left[f(t;k,m,\vec{\lambda})N_k(0)+g(t;k,m,\vec{\lambda})w_k\right] \qquad (19)
\end{aligned}
$$

$$
r(k,m,\vec{\lambda})=\begin{cases}\displaystyle\prod_{i=k,m-1}(b_{i+1}\lambda_i)\,, & \text{if } k<m\\ 1, & \text{if } k=m\end{cases} \qquad (20)
$$

$$
\begin{aligned}
&f(t;k,m,\vec{\lambda})\\
&\quad=(-1)^{m-k}\sum_{i=k,m}\left[\exp(-\lambda_it)\prod_{j=k,m;j\neq i}\left(\frac{1}{\lambda_i-\lambda_j}\right)\right] \qquad (21)
\end{aligned}
$$

$$
\begin{aligned}
&g(t;k,m,\vec{\lambda})=\frac{1}{\displaystyle\prod_{i=k,m}\lambda_i}+(-1)^{m-k+1}\\
&\quad\times\sum_{i=k,m}\left[\frac{1}{\lambda_i}\exp(-\lambda_it)\prod_{j=k,m;j\neq i}\left(\frac{1}{\lambda_i-\lambda_j}\right)\right]. \qquad (22)
\end{aligned}
$$

The set of equations below is used to calculate the amount of the $m$th isotope in the decay chain, where the $m$th isotope is stable.

$$
\begin{aligned}
&N_m(t;\vec{\lambda},\vec{b},\vec{w})=N_m+w_mt+\sum_{k=1,m-1}r(k;\vec{\lambda},\vec{b})\\
&\quad\times\left[f(t;k,m-1,\vec{\lambda})N_k(0)+g(t;k,m,\vec{\lambda})w_k\right] \qquad (23)
\end{aligned}
$$

$$
r(k,m,\vec{\lambda})=\begin{cases}\displaystyle\prod_{i=k,m-1}(b_{i+1}\lambda_i)\,, & \text{if } k<m\\ 1, & \text{if } k=m\end{cases} \qquad (24)
$$

$$
\begin{aligned}
&f(t;k,m,\vec{\lambda})=\frac{1}{\displaystyle\prod_{i=k,m}\lambda_i}+(-1)^{m-k+1}\\
&\quad\times\sum_{i=k,m}\left[\frac{1}{\lambda_i}\exp(-\lambda_it)\prod_{j=k,m;j\neq i}\left(\frac{1}{\lambda_i-\lambda_j}\right)\right] \qquad (25)
\end{aligned}
$$

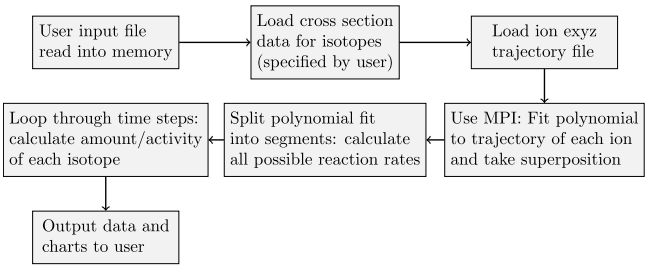


**Fig. 5.** Flow chart of major processes in the Activity code.

$$g(t;k,m,\vec{\lambda}) = \frac{1}{\prod_{i=k,m}\lambda_i}t + \frac{\sum_{i=k,m}\left[\prod_{j=k,m;j\neq i}\lambda_j\right]}{\prod_{i=k,m}\lambda_i^2} + (-1)^{m-k+1}\sum_{i=k,m}\left[\frac{1}{\lambda_i^2}\exp(-\lambda_i t)\prod_{j=k,m;j\neq i}\left(\frac{1}{\lambda_i-\lambda_j}\right)\right]. \quad (26)$$

### 1.10. Preference: analytic over numeric

The numeric solution only requires the equation to be solved in the s-domain; the Gaver–Stehfest algorithm performs the inversion. It is worth the extra effort to derive and implement an analytic solution, as the numeric is only an approximation. Examples of the pitfalls of the numeric solution are that it can give negative amounts of an isotope and the difference between the numeric and analytic calculated amounts can become quite large when the isotope decays away to a very small value. Fig. 4 shows the predicted decay of a sample of Po-218 irradiated for 1000 s, and sampled until 10,000 s. In the region between 4000 s and 9000 s the amount from the numeric calculation drops below zero, whereas the analytic calculation remains above zero, as would be expected.

## 2. Computational methods

The Activity program has been developed in Fortran and takes advantage of MPI (Message Parsing Interface) to speed up calculation times by allowing the use of multiple processes in parallel. It has a self contained maths library, although this could be improved in the future by using optimized maths libraries for certain functions (e.g. matrix operations).

The code was developed on a Debian based distribution of Linux, but it should be supported on other variants of Linux and Unix, and does not require any specialist hardware.

The user is required to prepare an input file that contains the instructions required to perform a calculation. In addition to the input file, the user must provide an EXYZ ion trajectory file output by SRIM. Activity will read in the user input file, and the SRIM and data files listed within, before performing the calculation. Fig. 5 shows a flowchart of the major steps the code performs.

There are various settings in the user input file, but the main ones relating to the simulated experiment are:

- Element composition of target (percentage by mass).
- Beam flux (current), energy, duration and area on target.
- Activity measurement time (end of the "experiment").
- Material density.
- Target thickness.

Several data files are generated by Activity and, if the user has matplotlib [7], charts will be created too. The most relevant to the user are:

- gammaLines.dat — tally into discrete bins of predicted gamma counts.
- ionTraj.dat — the averaged ion trajectory used in the calculation.
- isotopeActivityFileG.dat — a large data file detailing the activity of every predicted radioactive isotope in the target at user specified times following irradiation.

The charts include:

- activityTop5.png — activity of the top 5 active isotopes as a function of time after irradiation starts.
- gammaLines.png — predicted gamma spectrum expected at the "experiment end time".

The Activity code uses the equations derived above to calculate the amount and activity of each isotope in the calculation. One problem with the original Bateman equation that also exists in the set of modified Bateman equations is that two different isotopes with the same decay constant will cause a singularity and a halt in the calculation. The activity code loops through all the decay constants in use before it attempts to run the calculation. If any isotope decay constants match they are varied by a small amount relative to the decay constant. It repeats this process until all decay constants are unique before proceeding.

## 3. Approximations

The accuracy of the Activity code is dependent on the input files provided by the user and the method used to calculate the reaction rates and resulting activity. The TENDL proton database consists of experimental measured cross sections as well as values calculated using the optical model potential. Using the latest database is recommended.

SRIM uses the binary collision approximation to simulate ion transport. It is a well tested code that has been used for many years. One limitation is that the structure of the material is not taken into account. This would have an impact on a user of the Activity program if they were trying to calculate, for example, whether a FCC (face centered cubic) steel would be irradiated differently when compared to a BCC (body centered cubic) steel. The Activity code would determine the activity of the steel as a function of the ion current, ion type and the density, thickness and composition of the steel, not its structure.

This version of the Activity code averages the path of all the SRIM simulated ions, rather than treating each ion differently. This may or may not have an impact on the results. If a new version of the code is developed there would be an option to calculate reaction rates for each individual simulated ion, and a comparison could then be made to the calculations using the averaged path of a set of ions.

The final approximation would be to use the numeric solution to the activity equations, although the analytic solution is forced within the code unless it returns a failed result.

## 4. Results

A target of high purity Iron was irradiated with 36 MeV protons by the University of Birmingham Scanditronix MC-40 Cyclotron. The target was 0.5 mm thick and was irradiated at a current of 0.5 μA for 300 s, irradiating approximately 0.25 g of Iron. A high purity Germanium detector was used to measure the gamma peaks three days after irradiation.

The peak that dominated the readings was the 931 keV Cobalt 55 line. After calibrating the detector and adjusting the readings, this peak was measured at 44,300 Bq+/-2000 Bq. The activity of this peak as predicted by the Activity code was 44,565 Bq.

**Table 1**
Gamma peaks predicted and measured for a 13 MeV ion irradiated sample of Mo.

| Gamma energy (keV) | Predicted activity (Bq) | Experimental activity (Bq) |
|---|---|---|
| 766 | 4.45E6 | 5.11E5+/−2.5E4 |
| 778 | 6.14E6 | 1.36E6+/−6.8E4 |
| 812 | 5.04E6 | 1.15E6+/−5.8E4 |
| 850 | 6.00E6 | 1.39E6+/−7.0E4 |
| 126 | 9.33E5 | 2.10E5+/−1.1E4 |

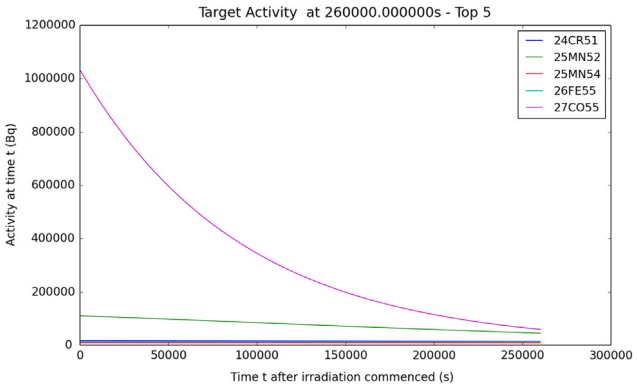


**Fig. 6.** Sample Activity code output chart for the top five most active isotopes for Iron irradiated by 36 MeV protons.

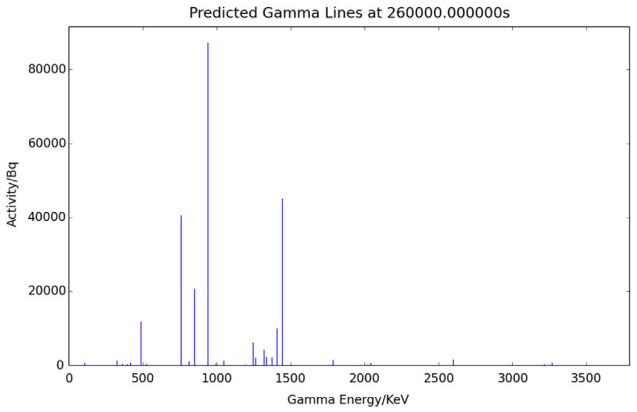


**Fig. 7.** Sample Activity code output chart for the expected gamma lines to be measured for Iron irradiated by 36 MeV protons.

A target of high purity Molybdenum was irradiated with 13 MeV protons by the University of Birmingham Scanditronix MC-40 Cyclotron. The target was 0.5 mm thick and was irradiated at a current of 5 μA for 1500 s, irradiating approximately 0.3 g of Molybdenum. A high purity Germanium detector was used to measure the gamma peaks three days after irradiation.

Five peaks were of interest, and these are listed in Table 1.

There was the possibility of the high purity Geranium detector introducing errors due to detector dead time, where by a source that is too active floods the device with gammas. The samples were safe to handle, and did not appear to flood the detector in any way, but there was still the possibility of counts being missed due to dead time. The probabilistic nature of radioactive decay also introduced inherent errors to the experimental activity measurements (see Figs. 6–9).

## 5. Conclusions

The Activity program is an easy to use Fortran compiled executable that can be built and run, for free, on a Linux computer. It takes advantage of multi-core processors, and typical calculations take from seconds to minutes.

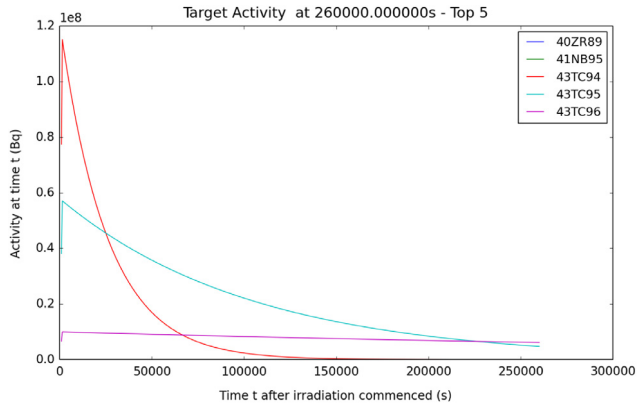


**Fig. 8.** Sample Activity code output chart for the top five most active isotopes for Molybdenum irradiated by 13 MeV protons.

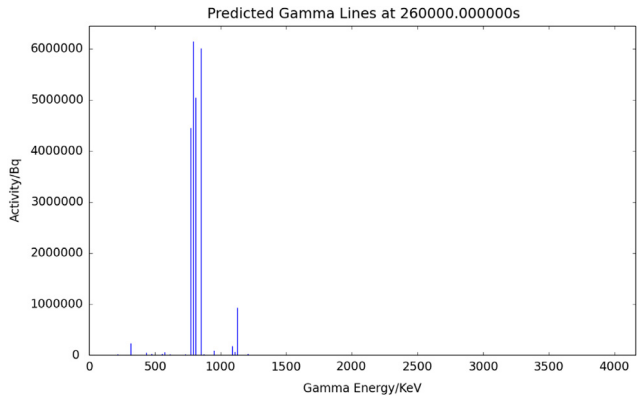


**Fig. 9.** Sample Activity code output chart for the expected gamma lines to be measured for Molybdenum irradiated by 13 MeV protons.

Using the SRIM code and TENDL database, the code has been used to predict the activity of Iron and Molybdenum targets that have been irradiated with a proton beam. The prediction of the 931 (keV) Cobalt 55 gamma activity of irradiated Iron was very close to the measured value. The five predicted gamma activities for ion irradiated Molybdenum were up to a factor of 5–10 away from the measured activities.

There are a number of improvements that would be considered in a future version of the Activity code. These improvements would include the following:

- A more readable output with less information printed, as too much may confuse the user.
- A file containing the top five radioactive isotopes with their top five gamma lines.
- Individual ion trajectories used to calculate the reaction rates, rather than the average path.
- Experimental ion activation data for a wider range of elements to test the Activity code against.
- Expand to include deuterons (this would require the TENDL deuteron cross section database).

## Acknowledgments

We would like to thank and acknowledge the input and advice of the following:

- Dr Chris Cooper and John Hewett for irradiation activation data points.

- The University of Birmingham for providing the funding for this project.

## References

[1] A.J. Koning, D. Rochman, Nucl. Data Sheets 113 (2012).
[2] A.A. Sonzogni, Nuclear Data Services. www-nds.iaea.org. 2006. URL: http://www-nds.iaea.org/ndspub/download-endf/ENDF-B-VII.0/decay-index.htm (visited on 08/14/2015).
[3] M. Herman, M.B. Chadwick, Nucl. Data Sheets 107 (2006) 2931.
[4] J.P. Biersack, J.F. Ziegler, M.D. Ziegler, Nuclear Instrum. Methods Phys. Res. B 268 (2010) 1818–1823.
[5] P. Blaise, M. Coste, A. Courcelle, T.D. Huynh, C. Jouanne, P. Leconte, O. Litaize, S. Mengelle, G. Nogure, J.-M. Ruggiri, O. Srot, J. Tommasi, C. Vaglio, J.-F. Vidal, A. Santamarina, D. Bernard, The JEFF-3.1.1 Nuclear Data Library. 2009. ISBN: 978-92-64-99074-6.
[6] H. Stehfest, Commun. ACM 13 (1970) 47–49.
[7] J.D. Hunter, Comput. Sci. Eng. 9 (2007) 90–95.

# Appendix D

# Activity Source Code

https://github.com/BenPalmer1983/activity

# Bibliography


[1] H. Khartabil. *Gen-4 Reactors*. 2013. URL: http://www.gen-4.org/GIF/About/documents/25-Session2-3-Khartabil.pdf (visited on 05/20/2013).

[2] MIT Open Courseware. *Engineering of Nuclear Systems - Lecture 6A*. 2013. URL: http://ocw.mit.edu/courses/nuclear-engineering/22-06-engineering-of-nuclear-systems-fall-2010/lectures-and-readings/MIT22_06F10_lec06a.pdf (visited on 05/20/2013).

[3] MIT Open Courseware. *Engineering of Nuclear Systems - Lecture 6B*. 2013. URL: http://ocw.mit.edu/courses/nuclear-engineering/22-06-engineering-of-nuclear-systems-fall-2010/lectures-and-readings/MIT22_06F10_lec06b.pdf (visited on 05/20/2013).

[4] E. Malambu A. Orden D. Struwe P. Agostini S. Monti A. Alemberti J. Carlsson. "European lead fast reactor - ELSY". In: *Nuclear Engineering and Design* 241 (2011), pp. 3470–3480.

[5] J. P. Biersack James F. Ziegler M. D. Ziegler. "SRIM - The stopping and range of ions in matter". In: *Nuclear Instruments and Methods in Physics Research Section B* 268 (2010), pp. 1818–1823.

[6] P. Blaise M. Coste A. Courcelle T.D. Huynh C. Jouanne P. Leconte O. Litaize S. Mengelle G. Nogure J-M. Ruggiri O. Srot J. Tommasi C. Vaglio J-F. Vidal A. Santamarina D. Bernard. *The JEFF-3.1.1 Nuclear Data Library*. 2009. ISBN: 978-92-64-99074-6.

[7] H. Stehfest. "Algorithm 368: Numerical Inversion of Laplace Transform". In: *Communications of the ACM* 13 (1970), pp. 47–49.